Muller, L. (1979) *J. Am. Chem. Soc. 101*, 4481.
Neri, D., Szyperski, T., Otting, G., Senn, H., & Wüthrich, K. (1989) *Biochemistry 28*, 7510.
Neri, D., Otting, G., & Wüthrich, K. (1990) *Tetrahedron 46*, 3287.
Nilges, M., Clore, G. M., & Gronenborn, A. M. (1988a) *FEBS Lett. 229*, 317.
Nilges, M., Clore, G. M., & Gronenborn, A. M. (1988b) *FEBS Lett. 239*, 129.
Olejniczak, E. T., & Eaton, H. L. (1990) *J. Magn. Reson. 87*, 628.
Olejniczak, E. T., Gampe, R. T. Jr., & Fesik, S. W. (1986) *J. Magn. Reson. 67*, 28.
Otting, G., & Wüthrich, K. (1989) *J. Magn. Reson. 85*, 586.
Otting, G., Senn, H., Wagner, G., & Wüthrich, K. (1986) *J. Magn. Reson. 70*, 500.
Quesniaux, V. F. J., Schreier, M. H., Wenger, R. M., Hiestand, P. C., Harding, M. W., & Van Regenmortel, M. H. V. (1987) *Eur. J. Immunol. 17*, 1359.
Quesniaux, V. F. J., Schreier, M. H., Wenger, R. M., Hiestand, P. C., Harding, M. W., & Van Regenmortel, M. H. V. (1988) *Transplantation 46*, 23S.
Rich, D. H., Sun, C.-Q., Guillaume, D., Dunlap, B., Evans, D. A., & Weber, A. (1989) *J. Med. Chem. 32*, 1982.
Rucker, S. P., & Shaka, A. J. (1989) *Mol. Phys. 68*, 509.
Senn, H., Werner, B., Messerle, B., Weber, C., Traber, R., & Wüthrich, K. (1989) *FEBS Lett. 249*, 113.
Shaka, A. J., Barker, P. B., & Feeman, R. (1985) *J. Magn. Reson. 64*, 547.
Sylvester, S. R., & Stevens, C. M. (1979) *Biochemistry 18*, 4529.
Takahashi, N., Hayano, T., & Suzuki, M. (1989) *Nature 337*, 473.
Weber, C., Wider, G., von Freyberg, B., Traber, R., Braun, W., Widmer, H., & Wüthrich, K. (1991) *Biochemistry*, preceding paper in this issue.
Wenger, R. (1983) *Transplant. Proc. 15*, 2230.
Wenger, R. M. (1985) *Angew. Chem. Int. Ed. Engl. 24*, 77.
Wider, G., Weber, C., Traber, R., Widmer, H., & Wüthrich, K. (1990) *J. Am. Chem. Soc. 112*, 9015.

Dynamics of the Quaternary Conformational Change in Trout Hemoglobin

James Hofrichter,* Eric R. Henry, Attila Szabo, Lionel P. Murray,‡ Anjum Ansari, Colleen M. Jones, Massimo Coletta,§ Giancarlo Falcioni,§ Maurizio Brunori,§,∥ and William A. Eaton

Laboratory of Chemical Physics, National Institute of Diabetes and Digestive and Kidney Diseases, National Institutes of Health, Bethesda, Maryland 20892

Received August 23, 1990; Revised Manuscript Received January 31, 1991

ABSTRACT: The kinetics of conformational changes in trout hemoglobin I have been characterized over the temperature range 2–65 °C from time-resolved absorption spectra measured following photodissociation of the carbon monoxide complex. Changes in the spectra of the deoxyheme photoproduct were used to monitor changes in the protein conformation. Although the deoxyheme spectral changes are only about 8% of the total spectral change due to ligand rebinding, a combination of high-precision measurements and singular value decomposition of the data permits a detailed analysis of both their amplitudes and relaxation rates. Systematic variation of the degree of photolysis was used to alter the distribution of liganded tetramers, permitting the assignment of the spectral relaxation at 20 μs to the R → T quaternary conformational change of the zero-liganded and singly liganded molecules and spectral relaxations at about 50 ns and 2 μs to tertiary conformational changes within the R structure. Analysis of the effect of photoselection by the linearly polarized excitation pulse indicates that a major contribution to the apparent geminate rebinding in the 50-ns relaxation arises from rotational diffusion of molecules containing unphotolyzed heme–CO complexes. The activation enthalpy and activation entropy for the $R_0 \rightarrow T_0$ transition are +7.4 kcal/mol and −12 cal mol^{-1} K^{-1}. Using the equilibrium data, ΔH = +29.4 kcal/mol and ΔS = +84.4 cal mol^{-1} K^{-1} [Barisas, B. G., & Gill, S. J. (1979) *Biophys. Chem. 9*, 235–244], the activation parameters for the $T_0 \rightarrow R_0$ transition are calculated to be $\Delta H^{\ddagger}$ = +37 kcal/mol and $\Delta S^{\ddagger}$ = +73 cal mol^{-1} K^{-1}. The similarity of the equilibrium and activation parameters for the $T_0 \rightarrow R_0$ transition indicates that the transition state is much more R-like than T-like. This result suggests that in the path from T_0 to R_0 the subunits have already almost completely rearranged into the R configuration when the transition state is reached, while in the path from R_0 to T_0 the subunits remain in a configuration close to R in the transition state. The finding of an R-like transition state explains why the binding of ligands causes much smaller changes in the R → T rates than in the T → R rates.

Upon deoxygenation tetrameric hemoglobins undergo a structural change consisting of a global rearrangement of the four subunits—the quaternary change—and widespread conformational changes within the individual subunits (Perutz, 1970; Baldwin & Chothia, 1979; Perutz et al., 1987). In the quaternary change the symmetrically related $\alpha\beta$ dimers rotate by about 15° relative to each other, resulting in atomic displacements at the intersubunit contacts of up to 6 Å (Baldwin & Chothia, 1979) (Figure 1). Recent X-ray studies also show that a change in ligation state in the absence of a quaternary conformational change results in tertiary conformational changes that are similar to, but smaller than, those associated with the quaternary transition (Makinen & Eaton, 1974;

* Author to whom correspondence should be addressed.
‡ Present address: Miles, Inc., Elkhart, IN 46515.
§ Permanent address: Department of Biochemical Sciences, University of Rome "La Sapienza", Piazzale A. Moro, 5, 00185 Rome, Italy.
∥ Fogarty Scholar-in-Residence, National Institutes of Health.

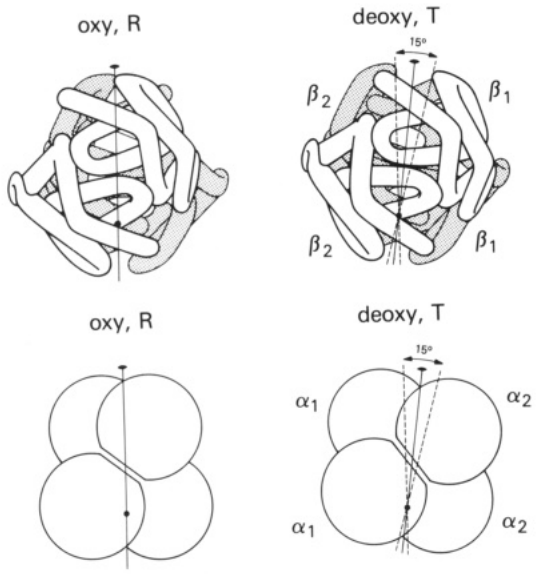

FIGURE 1: Schematic drawing of the change in quaternary structure of human hemoglobin [adapted from Dickerson and Geis (1983) and from Baldwin and Chothia (1979)]. The $\alpha_2\beta_2$ dimers in the two quaternary structures are superimposed, showing that the quaternary change consists mainly of a rotation of the $\alpha_1\beta_1$ dimer relative to the $\alpha_2\beta_2$ dimer by about 15°.

Perutz et al., 1987; Arnone et al. 1986; Liddington et al. 1988; Luisi & Shibayama, 1989).

In the two-state allosteric model for cooperative ligand binding there are only two quaternary structures—a high-affinity structure and a low-affinity structure (Monod et al., 1965). The key feature of the model is that the affinity of the hemes is determined by the quaternary structure, and not by the number of ligands bound to the tetramer per se (Shulman et al., 1975). This model not only provides a very good quantitative explanation for almost all of the equilibrium data on ligand binding (Shulman et al., 1975; Ackers & Smith, 1988) but has also provided the only useful framework for explaining a wide range of kinetic data (Hopfield et al., 1971; Sawicki & Gibson, 1976; Hofrichter et al., 1983; Marden et al., 1986; Murray et al., 1988a; Martino & Ferrone, 1989). In the kinetic formulation of the two-state model the overall rates of binding and dissociation depend only on the quaternary structure and not on the number of ligands that are already bound (Hopfield et al., 1971). There are no restrictions on the five R → T rates (one for each ligation state) or on the five T → R rates, apart from those imposed by the equilibrium constants (Figure 2).

Since the quaternary structural change plays a central role in our understanding of both kinetic and thermodynamic cooperativity, there have been several studies of quaternary transition rates (Sawicki & Gibson, 1976, 1977; Ferrone & Hopfield, 1976; Cho & Hopfield, 1979; Hofrichter et al., 1983, 1985; Ferrone et al., 1985; Marden et al., 1986; Murray et al., 1988a; Su et al., 1989; Martino & Ferrone, 1990). The measurements are difficult because the spectral changes resulting from the change in quaternary structure are much smaller than, and often totally obscured by, the spectral changes that result from ligand binding. Recent time-resolved optical spectroscopic experiments have highlighted the problem of measuring quaternary transition rates by revealing additional conformational relaxations on the time scale of 10 ns–1 μs with a spectral signature closely resembling that of the relaxation at later times which has been assigned to the R → T transition (Hofrichter et al., 1983, 1985; Murray et al., 1988a,b).

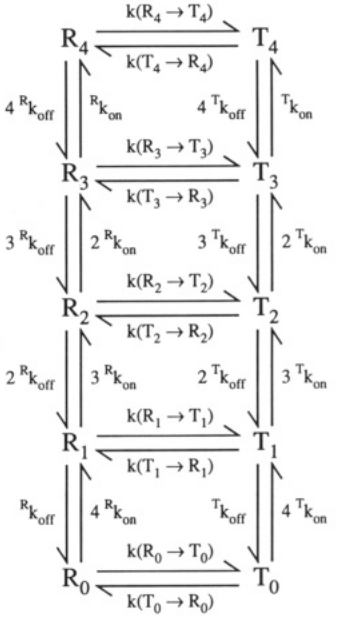

$$L_i = [T_i]/[R_i] = k(R_i \rightarrow T_i)/k(T_i \rightarrow R_i) = L_0 c^i$$

$$L_0 = [T_0]/[R_0]$$

$$c = (K_T/K_R) = ({}^{T}k_{on}/{}^{T}k_{off})/({}^{R}k_{on}/{}^{R}k_{off})$$

FIGURE 2: Two-state allosteric model. R and T refer to the quaternary structures of the stable fully liganded molecule and the stable fully unliganded molecule, respectively. The subscripts denote the number of ligands bound. The values of $L_0 = 3280$ and $c = 0.022$ were obtained by Barisas and Gill (1979) for the binding of carbon monoxide to trout Hb I at 20 °C. They indicate that at equilibrium zero-liganded and singly liganded molecules are in the T state, triply and quadruply liganded molecules are in the R state, and doubly liganded molecules are a 60/40 mixture of R and T.

The most unambiguous assignment of a heme spectral relaxation to an R → T quaternary transition has come from experiments in which the degree of photolysis of human (carbonmonoxy)hemoglobin was varied to produce differing distributions of liganded tetramers (Sawicki & Gibson, 1976, 1977; Hofrichter et al., 1983; Marden et al., 1986). Analysis of the amplitudes of the deoxyheme spectral changes as a function of the degree of photolysis led to the assignment of a relaxation at 20–200 μs (depending upon solution conditions) to the quaternary transition of the zero-liganded molecule. This assignment has been confirmed by several additional experiments. First, the time course of the deoxyheme spectral change is the same as the time course of the quenching of the fluorescence of 8-hydroxy-1,3,6-pyrenetrisulfonate (HPT), a dye that binds rapidly to the DPG pocket, signaling the rearrangement of the subunits to the T quaternary structure (Marden et al., 1986; Martino & Ferrone, 1989). Second, time-resolved ultraviolet resonance Raman measurements show spectral changes of aromatic residues simultaneous with the R → T deoxyheme spectral changes (Su et al., 1989), which are interpreted as resulting from changes in hydrogen bonding at the $\alpha_1\beta_2$ interface. Finally, the relaxation assigned to the R → T transition following photodissociation of a doubly liganded iron–cobalt hybrid molecule disappears upon switching this molecule to the T state with allosteric effectors (Murray et al., 1988a).

To extend our investigations of the kinetics of conformational changes in hemoglobin, we have undertaken a study of hemoglobin component I from trout (trout Hb I) (Brunori, 1975). This molecule was selected for a number of reasons.

Table I: Comparison of Residues in $\alpha_1\beta_2$ Contact in Human and Trout Hemoglobin[a]

	α Subunit														
Residue Number:	37	**38**	40	**41**	**42**	44	88	91	**92**	**94**	**95**	**96**	**97**	**140**	141
Human:	pro	**thr**	lys	**thr**	**tyr**	pro	ala	leu	**arg**	**asp**	**pro**	**val**	**asn**	**tyr**	arg
Trout:	pro	**gln**	lys	**thr**	**tyr**	ser	ala	leu	**arg**	**asp**	**pro**	**gly**	**asn**	**tyr**	arg

	β Subunit															
Residue Number:	34	35	36	**37**	**39**	**40**	**41**	**43**	**97**	98	**99**	100	**101**	**102**	105	145	146
Human:	val	tyr	pro	**trp**	**glu**	**arg**	**phe**	**gly**	**his**	val	**asp**	pro	**glu**	**asn**	leu	tyr	his
Trout:	val	tyr	pro	**trp**	**glu**	**arg**	**tyr**	**glu**	**phe**	val	**asp**	pro	**asp**	**asn**	val	tyr	phe

[a] Intersubunit contacts are those given by Perutz (1987). With the exception of β39 all of the listed residues are contacts in deoxyhemoglobin. The oxyhemoglobin contacts are listed in bold letters.

Most importantly, the thermodynamics of carbon monoxide binding to trout Hb I have been studied and analyzed in terms of the two-state allosteric model to produce enthalpies and entropies of ligand binding and the quaternary structural change (Wyman et al., 1977; Barisas & Gill, 1979). This allows us to combine the equilibrium parameters with activation parameters for the R → T transition to obtain activation parameters for the T → R transition of the zero-liganded molecule. The bimolecular kinetics of carbon monoxide binding to trout Hb I have also been investigated and found to be consistent with a two-state model (Brunori et al., 1980, 1982; Colosimo et al., 1982). The 50-fold faster overall association rate for the last carbon monoxide compared to the first indicates that kinetic cooperativity in this molecule is similar to that observed for human hemoglobin A (Brunori et al., 1980). Both the equilibrium binding curve and the overall association rate are independent of pH and anions (Binotti et al., 1971, 1973; Giardina et al., 1973; Wyman et al., 1977), eliminating possible heterotropic effects on the kinetics of conformational changes. Another useful characteristic of trout Hb I is that it is a more stable molecule than human hemoglobin. The tetramer–dimer dissociation constant for the fully liganded molecule has only been approximately measured (Brunori et al., 1973), but kinetic studies on dilute solutions show that no dimers are present, indicating that it must be less than 0.1 μM (Giardina et al., 1973; Airoldi et al., 1981). The molecule is also stable at temperatures as high as 65 °C for more than 1 h, permitting kinetic studies to be carried out over an extremely wide range of temperatures (Brunori et al., 1980, 1982). Finally, the interface between $\alpha\beta$ dimers is very similar in trout and human hemoglobin (Table I). Of the 31 residues in deoxyhemoglobin participating in intersubunit contacts between $\alpha\beta$ dimers (the $\alpha_2\beta_1$ and $\alpha_1\beta_2$ contacts), 24 are identical, and of the 18 residues in oxyhemoglobin 12 are identical. This sequence comparison suggests that the mechanism of the quaternary conformational change is very similar for the two molecules.

Materials and Methods

Sample Preparation. Trout hemoglobin I was prepared as described previously (Binotti et al., 1971) and was kept frozen until immediately prior to use. The samples were equilibrated with the final 0.1 M phosphate buffer, pH 7.0, by several cycles of concentration by pressure dialysis in a Centricon (Amicon), followed by redilution. The final sample was prepared by introducing a CO-saturated aliquot of the protein solution into a vial containing dry sodium dithionite (Virginia Chemicals) under a CO atmosphere. After addition of the hemoglobin solution the CO flux was maintained for at least 15 min under gentle stirring to ensure a final concentration of 1 mM free CO in solution. The sample (~0.1 mM in heme) was anaerobically loaded into a purged quartz EPR cell (0.34 mm, Wilmad), and the ends were sealed with dental wax and Glyptal varnish.

Measurement of Time-Resolved Spectra. Time-resolved absorption spectra were measured with a spectrometer which utilizes two Q-switched Nd:YAG lasers producing 10-ns (fwhm) pulses. The 532-nm second harmonic of the first (photolysis) laser (Quanta-Ray DCR-1A) was used to photolyze the hemoglobin sample. A second (probe) laser (Quanta-Ray DCR-1), which was electronically delayed with respect to the photolysis laser, was used to generate a "white" light flash which was used as the source for measuring the absorption spectrum of the sample. To do so, the third harmonic of the probe laser was cylindrically focused onto a 250-μm diameter capillary tube through which a solution of stilbene 420 in methanol was circulated by use of a peristaltic pump. The useful emission spectrum of this dye extends from 395 to 490 nm. The light from the dye cell was focused onto a slit-shaped volume of the sample which contained both a photolyzed and an unphotolyzed region and was subsequently refocused onto the 100-μm entrance slit of a 1/4-meter spectrograph.

The dispersed output from the spectrograph was collected on the faceplate of a silicon vidicon tube and read by an OMA detector controller (PAR 1216). To ensure linearity of the measured intensities, the vidicon target was repetitively scanned after each exposure to remove more than 98% of the charge. The controller was interfaced to a Hewlett Packard 9826 computer which had been programmed to collect, average, and store the data. The computer also controlled the timing of the laser shots and other tasks during data acquisition. Two tracks of intensities were measured, one from the photolyzed and one from the unphotolyzed region of the sample. The logarithm of the ratio of the two intensities at each wavelength produced a difference spectrum between the photoproduct and the unphotolyzed sample at a given time delay after photolysis.

The sample temperature was controlled by a specially constructed copper sandwich which enclosed the EPR cell and was connected to a brass heat-transfer block. The temperature of the block was controlled by a circulating bath. Dry nitrogen, equilibrated at the temperature of the brass block, was blown over the exposed surface of the cell to minimize gradients. The intensity of the photolysis laser was controlled by a pile-of-plates attenuator (Newport Corp.) and by varying the intensity of the flash lamp pumping the amplifier stage. The intensity

was monitored by an integrating diode detector (Molectron J3-05DW), and the measured voltage was digitized by an A–D converter.

Singular Value Decomposition of Data. Data from each experiment were analyzed by using singular value decomposition (SVD) as described previously (Hofrichter et al., 1985). This procedure rewrites the 480 × 100 data matrix, **A**, which consists of difference spectra measured at 480 wavelengths and 100 times, as a product of three matrices, $\mathbf{A} = \mathbf{USV}^T$. The matrix **U** is a 480 × 100 matrix of orthonormal basis spectra; **S** is a 100 × 100 diagonal matrix having all nonnegative elements, called the singular values of **A**; and **V** is a 100 × 100 orthogonal matrix in which each column of **V** describes the amplitude of the corresponding basis spectrum (column of **U**) at each of the 100 time delays. If the singular values are ordered by size, then the useful information from each experiment is contained in the first few columns of the **U** and **V** matrices. As a result, the SVD of the experiments was truncated to include only the first 12 columns of **U** and **V**. We estimate that less than 0.1% of the real kinetic and spectral information is lost as the result of truncation.[1] These truncated matrices provided a compact form in which to store the processed data for subsequent analysis.

To optimally extract the spectral information from the data sets collected at different degrees of photolysis, a global analysis was carried out to obtain a single set of basis spectra which could simultaneously describe all of the experiments. To do so, a data matrix **D** was assembled, which contained the observed spectra from all of the experiments. This data matrix described the sample absorbance as a function of the three independent variables: wavelength (λ), time (t), and degree of photolysis (x). The data for each of 13 (n_x) experiments were reconstructed from the truncated SVD of the original data. In reconstructing the data, the number of wavelengths (number of rows of the **U** matrix) was reduced to the resolution of the spectrograph (~1 nm) by smoothing the data with a Gaussian filter having a $1/e$ half-width of 2 pixels (0.4 nm) and interpolating the smoothed data onto an evenly spaced grid of wavelengths at 1-nm intervals. For each experiment the data were interpolated onto an identical set of time points $\{t_p\}$ after correcting for variations in the time at which the excitation laser pulse was generated, and the experimental points prior to the end of the photolysis pulse were deleted. Only the short time points are affected by the interpolation, since data at times longer than a few hundred nanoseconds were measured at the time delay onto which the interpolation was done. Smoothing and interpolation reduced n_λ from 480 to 83, and interpolation on the time axis reduced n_t from about 100 to 89. The data matrix **D** thus contained 83 × 89 × 13 (96031) data points, roughly 1/6 of the original 480 × 100 × 13 (624000) data points. The data in **D** are arranged as n_λ rows by ($n_t \times n_x$) columns; each column of **D** contains a single reconstructed spectrum corresponding to a specific degree of photolysis (x) and a single time delay (t).

SVD was again used to extract the minimal set of linearly independent basis spectra which describe all of the data at different degrees of photolysis, i.e.

$$\mathbf{D} = \mathbf{USV}^T \tag{1}$$

This procedure expresses the complete λ, t, and x dependences of **D** as sums of products of (λ-dependent) basis spectra and (t- and x-dependent) amplitudes. The matrix **U**, in this case, is an $n_\lambda \times n_\lambda$ (83 × 83) matrix of basis spectra, **S** is an $n_\lambda \times n_\lambda$ (83 × 83) diagonal matrix of nonnegative singular values, and **V** is an $(n_t \times n_x) \times n_\lambda$ [(89 × 13) × 83] matrix, each column of which describes the amplitude of the corresponding column of **U** for all degrees of photolysis (x) and times (t). It was possible to discriminate against random sources of experimental "noise" which are wavelength correlated but are uncorrelated with the time delay between the excitation and probe pulses by using a procedure that minimizes the high-frequency noise components in the retained columns of **V**. This was accomplished by a transformation of the **V** matrix so as to optimize the autocorrelations of the retained column of **V**. The major source of such noise in these experiments was base line offsets arising from shot-to-shot variation in the distribution of output energy in the probe laser pulse.

The transformation is mathematically represented in terms of the orthogonal matrix **R** (i.e., $\mathbf{R}^{-1} = \mathbf{R}^T$) as

$$\mathbf{D} = (\mathbf{USR})(\mathbf{VR})^T = (\mathbf{U}^R)(\mathbf{V}^R)^T \tag{2}$$

The procedure for obtaining the matrix **R** is described elsewhere (Henry & Hofrichter, 1991). This procedure generated a new set of basis spectra

$$\mathbf{U}^R = \mathbf{USR} \tag{3}$$

which are still linearly independent, but no longer orthonormal. The matrix

$$\mathbf{V}^R = \mathbf{VR} \tag{4}$$

describes each of the measured spectra in terms of the basis spectra in $\mathbf{U}^R$. The transformation preserves the orthogonality of the **V** matrix. In applying this procedure, the first column of **V** was excluded from the optimization procedure (i.e., not transformed) because the first singular value was more than 20 times larger than the second. The small relative amplitudes of the additional singular values guarantee that the first column of **V** provides a good first approximation to the ligand rebinding curve (Hofrichter et al., 1983, 1985; Murray et al., 1988a), and it is useful to retain this feature in the transformed basis spectra. The transformation of the **V** matrix was applied to components 2–12, none of which represented real spectral changes which were larger than about 4 times the largest instrument noise component.

Following this procedure, the transformed **U** and **V** matrices ($\mathbf{U}^R$ and $\mathbf{V}^R$) were truncated to include only the highly time-correlated components. The truncated and transformed SVD representation of the data contained four basis spectra (columns of $\mathbf{U}^R$) of 83 points each and four amplitude vectors (columns of $\mathbf{V}^R$) of 89 × 13 = 1157 points each, so all of the useful information in the 96031 elements of the matrix **D** has been represented with only the 4 × (83 + 1157) = 4960 elements of $\mathbf{U}^R$ and $\mathbf{V}^R$, a compression of approximately 20-fold.

Fitting the Data with Exponential Relaxations. Many systems can be described by kinetic models which produce a set of coupled linear differential equations with time-independent coefficients. Since the solutions to these equations are sums of exponential relaxations, the data can be empirically

[1] If the singular values of the discarded components are used to quantitate the differences, approximately 1% of the original data is discarded by truncation to retain only the first 12 SVD components. However, a large fraction of the amplitude of the discarded components arises from fluctuations that are much too rapid to represent real changes in the spectra or populations of the photoproducts. If it is assumed that real spectral and kinetic information is represented by amplitudes which are correlated over more than 5 nm and more than a half decade in time, the norms of the higher SVD components are reduced by more than a factor of 10 relative to those of components 1–4, arguing that the amount of real spectral and kinetic information lost by truncation is less than 0.1%.

analyzed by fitting with sums of exponential relaxations. If applied directly to the data matrix **D**, this procedure would describe each of the $n_\lambda \times n_x$ time-dependent vectors by a sum of exponentials. The total number of parameters required to describe **D** would therefore be $(n_\lambda \times n_x + 1) \times n_k$, where n_k is the number of exponential relaxations, and it is assumed that the number of relaxations and the relaxation rates are the same at each wavelength for all degrees of photolysis. The SVD procedure provides an immediate dividend in carrying out such an analysis. Since all of the wavelength dependences of the data are represented in terms of the n_u (=4) retained basis spectra, the data at all n_λ wavelengths can be fit by considering only the n_u columns of the $\mathbf{V}^R$ matrix, that is, by fitting $n_u \times n_x$ (4 × 13) time-dependent vectors, instead of $n_\lambda \times n_x$ (83 × 13) vectors. In carrying out the fits, the number of components is further reduced by using SVD to decompose the individual vectors V^R_i, each of which contains the time-dependent amplitudes of a single basis spectrum U^R_i for all degrees of photolysis. Each of these n_u vectors is rearranged to produce an $n_t \times n_x$ matrix ${}^i\mathbf{V}$ ($i = 1, ..., n_u$), with $({}^i\mathbf{V})_{pq} = (V^R_i)_{(q-1)n_t+p}$, for $p = 1, ..., n_t$ and $q = 1, ..., n_x$. Each column of ${}^i\mathbf{V}$ thus contains the time-dependent amplitudes of basis spectrum U^R_i for a single degree of photolysis. Each matrix ${}^i\mathbf{V}$ is decomposed by SVD as

$$ {}^i\mathbf{V} = {}^i\mathbf{X}\,{}^i\mathbf{Y}({}^i\mathbf{Z})^T \quad (5) $$

This effectively separates the t and x dependences of the amplitude vector V^R_i into sums of products of time-dependent vectors (columns of ${}^i\mathbf{X}$) and photolysis-dependent amplitudes (elements of ${}^i\mathbf{Z}$). In this way the original λ, t, and x dependences of the data matrix **D** have been separated into distinct wavelength dependences (basis spectra U^R_i), time dependences (elements of the matrices ${}^i\mathbf{X}$), and photolysis dependences (elements of the matrices ${}^i\mathbf{Z}$). The decomposition of the four ${}^i\mathbf{V}$ matrices obtained from the measurements on trout hemoglobin I provided a set of time-dependent vectors, the columns of ${}^i\mathbf{X}$, which describes the amplitudes of the four basis spectra U^R_i for all sets of experimental conditions.[2] For the partial photolysis data, the numbers of columns of the matrices ${}^i\mathbf{X}$ which had amplitudes corresponding to more than 0.2% of the total amplitude of the data set and exhibited sufficient signal to noise to justify fitting were 2 for ${}^1\mathbf{X}$ (i.e., $i = 1$), 2 for ${}^2\mathbf{X}$, 2 for ${}^3\mathbf{X}$, and 3 for ${}^4\mathbf{X}$, reducing from 4 × 13 = 52 to only 9 the number of independent vectors that had to be simultaneously fit to describe the data. In fitting the data, the jth column of ${}^i\mathbf{X}$ was weighted by the product of the norm of U^R_i (the equivalent of the singular value in the absence of rotation) and $({}^i\mathbf{Y})_{jj}$, the singular value obtained from the SVD of ${}^iV$. This weighting is analogous to the weighting by singular values that has been previously suggested (Shrager, 1986).

The selected columns of the ${}^i\mathbf{X}$ were then fit with sums of exponential relaxations. We utilized a previously suggested procedure (Mauer et al., 1987; Hofrichter et al., 1989) in which the fit was first carried out for a small number of relaxation rates, typically 3 or 4, with a number of different sets of initial conditions. The rates and amplitudes were optimized from each set of initial conditions. The rates that produced the best fit for a given number of relaxations, plus an additional rate, were used as initial conditions for a series of fits to the next larger number of relaxations. For these fits, an initial value of the additional rate was chosen in each of the possible ordered positions relative to the remaining rates provided by the previous set of fits. This procedure was continued until the improvement in the fits was negligible or until the fits no longer converged when a new relaxation was introduced. Each fit produced a set of relaxation rates, k_r ($r = 1, ..., n_k$), and a set of amplitudes, f_{ijr}, which describe the changes in the jth column of ${}^i\mathbf{X}$ which take place with relaxation rate k_r. The fit to ${}^i\mathbf{X}$ can then be written

$$ ({}^i\mathbf{X})_{pj} \simeq \sum_r f_{ijr} \exp(-k_r t_p) \quad (6) $$

where $\{t_p\}$ ($p = 1, ..., n_t$) is the set of interpolated time points used in analyzing the data for all conditions. The matrix $\mathbf{U}^R$ and the set of fit coefficients f_{ijr}, together with the set of rates k_r, provide an extremely compact representation of the experimental data. The total number of parameters required to represent the 96 031 points in the interpolated data matrix is 402 (four 83-wavelength basis spectra from $\mathbf{U}^R$; 7 relaxation rates, k_r; 63 fit coefficients, f_{ijr}).

The fit coefficients f_{ijr} can now be used to generate the corresponding fitted amplitudes which describe the spectral changes taking place in each relaxation, r, in terms of the global basis spectra, $\mathbf{U}^R$. We first generated the fitted approximation to the four matrices, ${}^i\mathbf{V}$, which describe the amplitudes of the original data. Using eqs 5 and 6, we obtain

$$ ({}^i\mathbf{V})_{px} \simeq \sum_r g_{ixr} \exp(-k_r t_p) \quad (7) $$

where

$$ g_{ixr} = \sum_m f_{imr} ({}^i\mathbf{Y})_{mm} ({}^i\mathbf{Z})_{xm} \quad (8) $$

Then, taking into account the fact that the matrices ${}^i\mathbf{V}$ are simply rearrangements of the original amplitude vectors V^R_i, we derive the fitted amplitudes for the change in the photoproduct spectrum which takes place during relaxation r for degree of photolysis x from eq 2:

$$ (\Delta OD)_{\lambda xr} = \sum_i U^R_{\lambda i} g_{ixr} \quad (9) $$

The coefficients g_{ixr}, defined by eq 8, describe the amplitudes of each of the basis spectra for each relaxation and set of conditions.

We also used SVD to examine the dependence of these spectral changes on composition. SVD is an efficient algorithm for both averaging and determining the rank of the difference spectra for a specific relaxation r. This can be done in a very compact form, since the spectra are represented as linear combinations of the basis spectra, U^R_i. To do so, the matrix ${}^r\mathbf{G}$ was formed from the subset of the coefficients g_{ixr} for each relaxation r [i.e., $({}^r\mathbf{G})_{ix} = g_{ixr}$], and the SVD of ${}^r\mathbf{G}$ was calculated. ${}^r\mathbf{G}$ is the matrix of coefficients of the U^R_i which describes the spectral change during relaxation r for each degree of photolysis, x. If all of the difference spectra associated with a given relaxation are multiples of a single spectrum, then the rank of ${}^r\mathbf{G}$ as determined from the SVD will be 1. If more than a single spectrum is required to describe the spectra, the rank will be higher than 1. It should be noted that since there are only four basis spectra, the rank of any observed set of spectral changes must be 4 or less.

Results

The data reported here were obtained from a set of 29 experiments. In each experiment spectra were measured at approximately 100 different time delays spaced on a logarithmic grid from coincidence between the 10-ns excitation and probe pulses to the completion of ligand rebinding. Each spectrum was the difference in optical density between the photolyzed sample and the fully liganded sample, which was

[2] In the case of the partial photolysis experiments, the rank of the matrix ${}^i\mathbf{V}$ must be equal to or less than the number of independent photoproduct species, n_s. This decomposition therefore reduces the number of vectors which must be fit to less than $n_u \times n_s$.

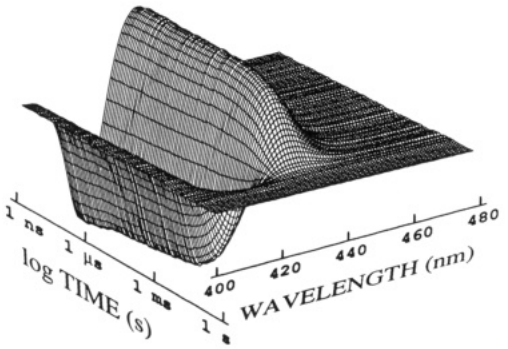

FIGURE 3: The data (**A**) from a maximum photolysis experiment at 20 °C. The sample was photodissociated by using the maximum laser power employed in the experiments. The measured difference in optical density between the photoproduct and the unphotolyzed sample is displayed as a function of wavelength and time (on a logarithmic scale). A total of 89 measured spectra, consisting of optical density differences at each of 480 wavelengths, are shown after being smoothed by convolution with a Gaussian having a half-width at $1/e$ of 2 channels. After smoothing, the data were sampled at 1-nm intervals from 398 to 480 nm.

used as a reference, at a total of 480 wavelength points between 395 and 490 nm. Each spectrum was obtained from the sum of intensities from 21–30 laser shots. A series of 16 experiments was carried out at temperatures from 2 to 65 °C in which the sample was maximally photolyzed. Additional experiments were performed at 20 °C after exposure of the sample to 42 and 65 °C to ensure sample integrity. A second series of 13 experiments was carried out at 20 °C in which the energy of the photolysis pulse was adjusted so as to vary the fraction of hemes dissociated from about 0.1 to 0.9. The results of these partial photolysis experiments were used to determine which of the observed relaxations contained a quaternary structural change. The temperature dependence of the kinetics was also examined in an earlier set of 7 experiments on a totally independent preparation which yielded essentially identical results.

Figure 3 shows a three-dimensional plot of the data from a maximum photolysis experiment at 20 °C. The singular value decomposition (SVD) of this data is shown in Figure 4. The basis spectrum with the largest singular value, U_1, is the deoxy – CO difference spectrum which produces the best one-component least-squares fit to the data. Because the spectral changes represented by the higher SVD components are small, the vector V_1, which describes the time course of the amplitude of this basis spectrum, provides a very good measure of the fraction of the sample that is unliganded. The higher SVD components (U^R_2 and V^R_2 and U^R_3 and V^R_3) represent changes in the spectra of the deoxyhemes generated by photolysis, as well as much smaller differences between the spectra of the liganded hemes in photodissociated tetramers and the spectrum of the equilibrium liganded species. The maximum amplitude of the spectral changes described by U^R_2 and V^R_2 is only about 0.05 OD unit. Comparison of this amplitude with that of the deoxy – CO difference spectrum (0.72 OD unit) shows that the spectral perturbations observed in this experiment represent changes of only a few percent in the extinction coefficients of the photoproduct.

Partial Photolysis Experiments. As pointed out in the introduction, to determine whether a relaxation results from a quaternary conformational change, it is necessary to measure how the amplitude of the spectral changes depends on the fraction of heme–CO complexes photodissociated by the excitation pulse. It is not straightforward to obtain the amplitude information from independent fits to individual data sets,

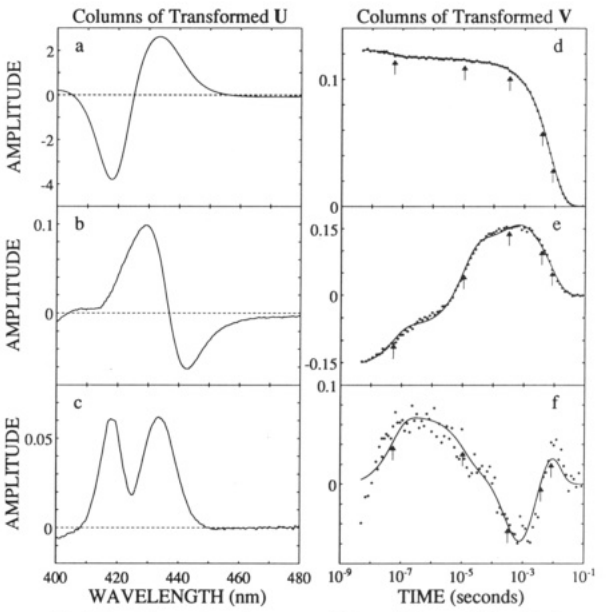

FIGURE 4: Singular value decomposition of data (**A**) which was smoothed to obtain Figure 3. The first 3 columns of the transformed **U** (panels a–c) and **V** (panels d–f) matrices are shown. The amplitudes of the remaining columns of the transformed **U** matrix, multipled by the corresponding column of the transformed **V**, are smaller at all time delays than the noise in the measurement. The fit of the 3 columns of the transformed **V** matrix to a sum of 5 exponential relaxations is shown as the continuous curves in panels d–f. The relaxation times are indicated by the arrows.

Table II: Relaxation Rates Obtained from Fits of Partial Photolysis Data at 20 °C to Sums of Exponential Relaxations

relaxation	rate (s^{-1})	rate (s^{-1})	rate (s^{-1})	rate (s^{-1})
I	2.0×10^7	2.0×10^7	1.8×10^7	1.7×10^7
II	6.0×10^5	6.0×10^5	1.0×10^5	5.2×10^4
III	4.7×10^4	4.7×10^4	2.1×10^3	8.3×10^2
IV	2.7×10^3	2.3×10^3	3.8×10^2	1.4×10^2
V	6.8×10^2	3.8×10^2	1.3×10^2	
VI	3.6×10^2	1.3×10^2		
VII	1.2×10^2			
final sum of squares	0.0175	0.0190	0.0225	0.0457

because the fitted amplitudes are dependent on the relaxation rates and the best-fit relaxation rates depend systematically on the extent of photolysis. To overcome this problem, we carried out a global analysis of the partial photolysis data sets using the procedure described under Materials and Methods. This analysis produced a set of relaxation rates which best fit the data over the complete range of fractional photolysis and the spectral changes associated with these relaxations described in terms of the global basis spectra ($\mathbf{U}^R$) shown in Figure 5. The fits converged up to a total of 7 relaxations, and the best-fit rates and the final sums of squared residuals are given in Table II.

The fit to 4 relaxations includes the bimolecular binding relaxation seen as most prominent in Figures 3 and 4 at about 7 ms, a second ligand rebinding relaxation at about 1 ms, required to fit the ligand binding amplitudes at low extents of photolysis, a relaxation at about 20 μs which arises primarily from the second SVD basis spectrum, and a rapid relaxation which includes geminate rebinding at about 60 ns. These 4 major relaxations are resolved in all of the fits (Table II). As we shall see below, the 20-μs relaxation results from the change in quaternary conformation from R to T, so it is clear that this relaxation is one of the major features of the data and the determination of its relaxation rate is not dependent on the exact number of relaxations chosen for the analysis. On the

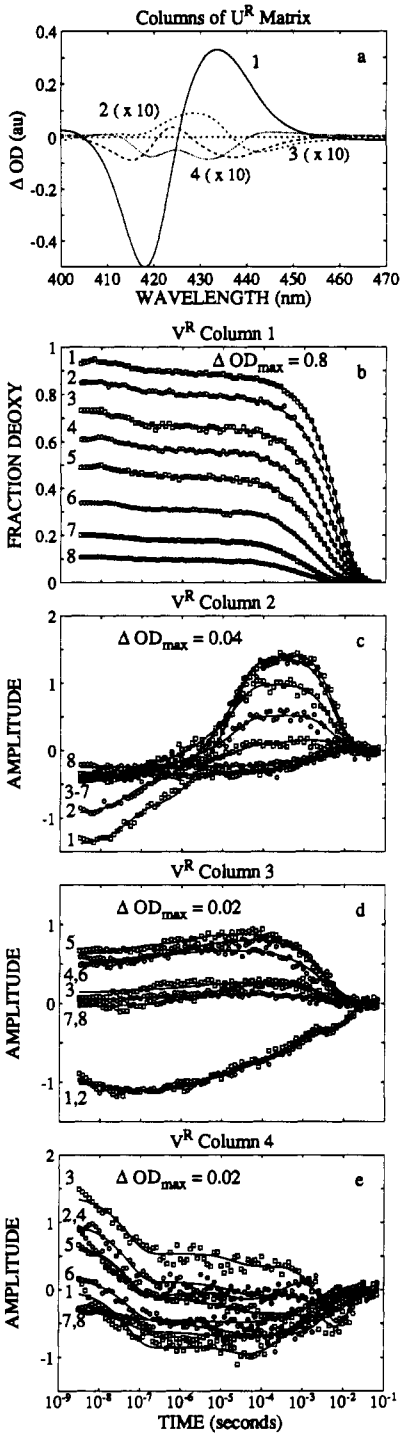

FIGURE 5: SVD analysis of the partial photolysis experiments at 20 °C. The output of the transformed SVD included 4 basis spectra. (a) The U^R matrix obtained from the SVD analysis of the partial photolysis experiments (**D**). The first four columns of the matrix are the basis spectra which correspond to the amplitudes in (b), (c), (d), and (e). (b–e) The points are the portion of the ^fV matrices that result from 8 of the 13 experiments. Each ^fV has been multiplied by a factor of 16.3, so that the elements of ^1V closely approximate the fraction of deoxyhemes. SVD of the four ^fV matrices produced a total of 9 significant vectors which were fit with sums of exponentials. The numbers of vectors required to represent ^1V, ^2V, ^3V, and ^4V were 2, 2, 2, and 3, respectively. The curves are the fitted amplitudes for the 8 plotted experiments obtained from the weighted fit of all of the data to sums of seven exponential relaxations using eq 6 (see Materials and Methods). The curves are calculated from eq 7 using the fit coefficients, f_{ij}, and the relaxation rates in Table II. The ΔOD_{max} for each SVD component is the maximum OD minus the minimum OD multiplied by the element of the ^fV matrix with the largest absolute value.

basis of the decrease in the final sum of squares, the fit to 7 relaxations was selected and the remainder of our analysis of the partial photolysis data is based on the results of this fit.

To assign these 7 relaxations to molecular processes, we need to know not only the relaxation rates but also how the amplitudes and shapes of the difference spectra depend on the degree of photolysis. In particular, it is useful to know how many different spectral components are necessary to fit the difference spectra observed for each relaxation. If a given relaxation corresponds to a single molecular process, for example the $R_0 \rightarrow T_0$ transition, then its spectrum should be the same at all degrees of photolysis and only its amplitude should vary. The difference spectra measured as a function of the extent of photolysis should then be describable in terms of a single difference spectrum; the matrix of these spectra will contain only a single linearly independent component, i.e., have a rank of 1. More complex processes might also appear as rank 1 if they produce spectral changes that are identical at all degrees of photolysis. If, on the other hand, a relaxation contains contributions from two or more processes that have different spectral signatures and scale differently with the extent of photolysis, but happen to take place on the same time scale, then more than one spectrum will be required to fit the spectra observed for this relaxation and the rank will be higher than 1. The most straightforward way to determine the rank of the spectral changes occurring in each relaxation is, again, to use SVD. Clearly, an observed rank higher than 1 means that more than a single process is occurring in a given relaxation.

The SVD analysis of the spectral changes observed for relaxations I–VII is shown in Figure 6. The results show that relaxations I, III, IV, and VII are very close to rank 1, whereas relaxations II, V, and VI are rank 2. In the case of relaxation II, the total magnitude of the spectral changes is so small that the second component amounts to absorbance changes of only 0.003 OD, while the second components for relaxations V and VI are more than an order of magnitude larger. Because its amplitude is so small, we shall ignore the second component for relaxation II and treat this relaxation as rank 1 in the following discussion.

The next step is to analyze the difference spectra obtained for these relaxations in terms of contributions from ligand rebinding, deoxyheme spectral changes, and other spectral contributions. To highlight the problems in carrying out these assignments, the spectra prior to each relaxation are compared in Figure 7a. Since the difference spectra observed before each of the intermediate relaxations fall between these two extreme spectra, it is obvious that we are analyzing difference spectra that are only perturbations on the average deoxy – CO difference spectrum. The spectral changes which correspond to the amplitudes in Figure 6, panels a, b, and c, for relaxations I, II, and III have amplitudes of only about 0.04, 0.008, and 0.015 OD units, respectively.

The spectral changes for relaxations I, II, and III are shown in Figure 7, panels b, c, and d. Each of these difference spectra is very different from (the negative of) any of the deoxy – CO difference spectra for the photoproduct shown in Figure 7a. It is clear, therefore, that these relaxations cannot be explained as simple ligand-rebinding relaxations. Each must include a process that produces a change in the spectrum of the deoxy (and perhaps also of the liganded) hemes of the photoproduct molecules. The contribution from the deoxy hemes must dominate since each amplitude scales monotonically with the extent of photolysis (Figure 6a–c).

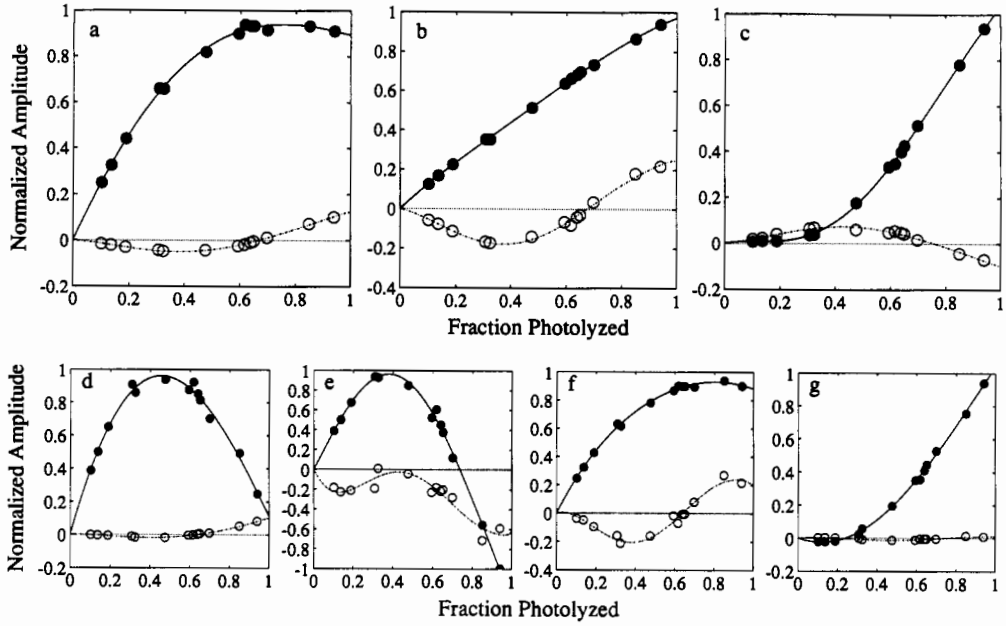

FIGURE 6: Dependence of the spectral changes observed for each of the seven exponential relaxations on the degree of photolysis. Singular value decomposition was used to determine the amplitudes of the spectral changes occurring in each relaxation and their dependence on the extent of photolysis (see Materials and Methods). (a–g) Amplitudes of the first two components of the spectral changes for relaxations I–VII, respectively; (filled circles) first component and (open circles) second component. In each case the results have been normalized by arbitrarily setting the maximum amplitude of the first component to 0.94, the estimated maximum extent of photolysis. The maximum amplitudes prior to normalization were 0.104, 0.027, 0.060, 0.123, 0.099, 0.379, and 1.25 for relaxations I–VII, respectively. The lines are empirical fits to the data.

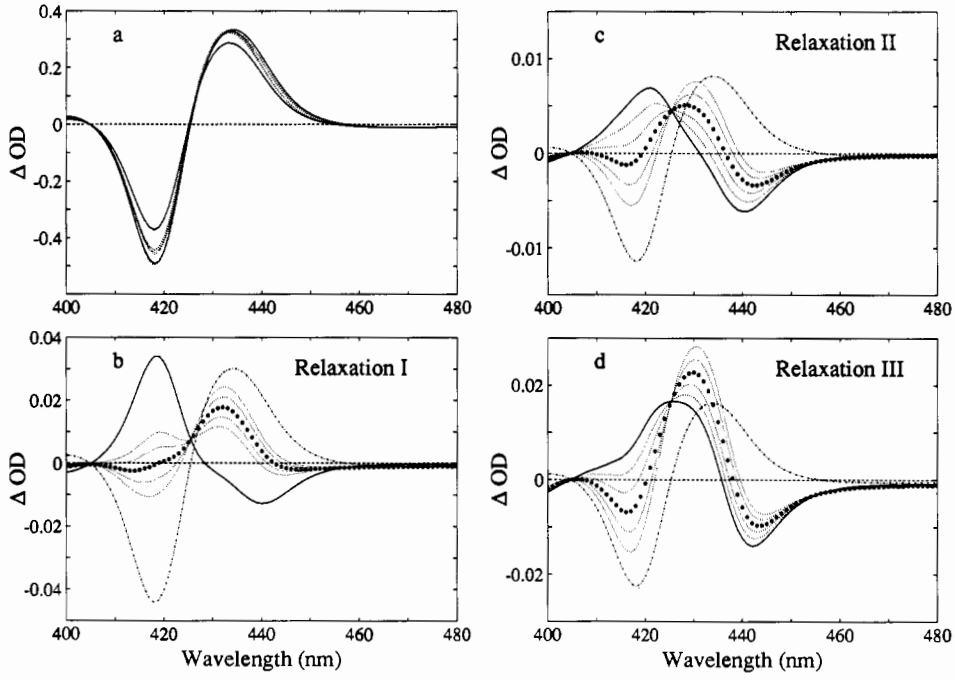

FIGURE 7: Spectral changes observed for relaxations I–III. The spectral change occurring in each relaxation was obtained by using eq 9 after extrapolating the first two components of the SVD analysis of 'G shown in Figure 6 to 100% photolysis. The deoxy – CO difference spectra prior to each relaxation were obtained by the same procedure. (a) The extrapolated deoxy – CO difference spectra observed prior to each of the seven relaxations. The continuous curves are the spectra prior to relaxations I and VII. The dotted curves are the difference spectra prior to relaxations II–VI. (b–d) Spectral changes accompanying relaxations I–III and their decomposition into CO – deoxy difference spectra due to CO rebinding and deoxy spectral changes. The spectral change for relaxation r is equal to the difference spectrum prior to relaxation $r + 1$ minus the difference spectrum prior to relaxation r. The continuous curve is the spectral change at 100% photolysis. The dashed-dotted curve is the deoxy – CO difference spectrum prior to each relaxation, scaled to correspond to the largest of the corrected amplitudes for each relaxation. The heavy dotted spectra are the best estimates of the deoxyheme spectral changes, assuming that there is no spectral change of the CO–hemes. The changes in fractional saturation associated with the corrections were 0.07 for relaxation I (b), 0.015 for relaxation II (c), and 0.03 for relaxation III (d). The dotted curves are the deoxyheme spectral changes obtained by varying the change in fractional saturation about these values. The change in fractional saturation between each curve is 0.01 for relaxations I (b) and III (d) and 0.005 for relaxation II (c).

From the data in Figures 6 and 7 there is no way to uniquely determine the changes in the spectra of the deoxy photoproduct which take place in these relaxations, since the change in fractional saturation cannot be unambiguously determined. Since we are considering only the rank 1 component of these 3 relaxations, there is no significant difference among the

spectral changes observed at all degrees of photolysis. Consequently, any linear combination of this spectrum and the CO – deoxy spectrum is a possible description of the spectral change resulting from the deoxy hemes. It is important to point out that this problem in no way affects the assignment of these relaxations on the basis of the dependence of their amplitudes on the extent of photolysis. If the observed spectral changes can all be represented by a single spectrum (i.e., if the rank of the set of spectra is 1), then the amplitude of the deoxy spectral change will scale with the amplitude of the measured difference spectra, independent of the amount of ligand rebinding assigned to the relaxation. It is reasonable to rule out candidate spectra that closely resemble the deoxy – CO difference spectrum but, since many of the possible deoxy difference spectra include a negative spectral feature at wavelengths close to the peak absorption of the heme–CO complex, it was not possible to use the amplitude of this feature to unambiguously remove the CO peak from the deoxy difference spectra [cf. Hofrichter et al. (1985)]. Figure 7b–d presents our best guesses for the deoxy spectral changes, together with some alternative possibilities which differ only by admixture of different amounts of the deoxy – CO difference spectrum. Our best guesses for relaxations II and III produce deoxyheme spectral changes which describe a sharpening of the deoxy spectrum without a significant increase in its integrated extinction coefficient. For relaxation I, however, it was impossible to subtract any CO – deoxy difference spectrum and obtain a deoxy difference spectrum which did not have either a large increase in integrated extinction coefficient or a significant negative peak near the peak absorbance of the CO-liganded heme.

Temperature Dependence in Maximum Photolysis Experiments. The dependence of the kinetics on temperature was investigated in a series of maximum photolysis experiments carried out over a range from 2 to 65 °C. The relaxation rates between 10^4 and 10^8 s^{-1} obtained from the fits to these data are shown in Figure 8a. The interpretation of these results is complicated by the fact that the amplitudes of the spectral changes, and hence the ability to time-resolve them, decrease as the temperature increases. At temperatures below 25 °C, five exponential relaxations are required to fit the data, while at higher temperatures, only four relaxation rates can be resolved. The additional relaxation is that which appeared as relaxation II in the fits to the partial photolysis data at 20 °C. It is not possible from the results to determine unambigously whether the single submicrosecond relaxation observed at the higher temperatures corresponds to relaxation II at the lower temperatures or really contains contributions from two relaxations which are not resolved because the associated amplitudes are too small (see Figure 8b,c). The temperature dependence of the amplitudes was determined in the same way as in the partial photolysis experiments (Figure 6). That is, the spectral changes associated with each of the relaxations were analyzed by SVD. The amplitudes of the rank 1 and rank 2 components for relaxations I–III are shown in Figure 8b,c.

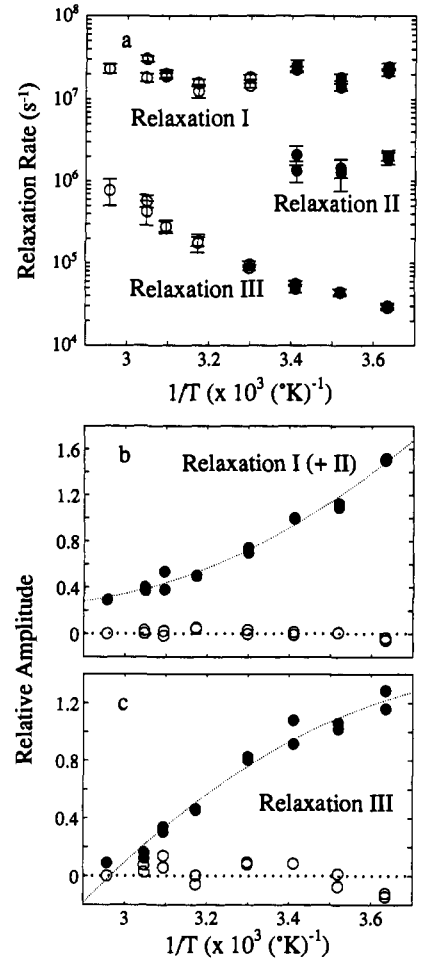

FIGURE 8: Temperature dependence of relaxation rates and amplitudes of spectral changes in relaxations I–III. (a) Arrhenius plot of relaxation rates from maximum photolysis experiments. Data sets measured at 20 °C and below were fit by using five exponential relaxations, and the fitted rates for the first three relaxations are shown as the filled circles. Data sets measured at temperatures above 20 °C were fit with four exponential relaxations, and the rates for the first two are shown (open circles). (b) Temperature dependence of the amplitude of tertiary relaxations. The amplitude of the spectral change observed in relaxation I (above 20 °C) or relaxation I + relaxation II (20 °C and below) is plotted as a function of the reciprocal temperature. The amplitudes (filled circles) were determined from the first component of the SVD analysis of the set of spectral changes. The relative magnitudes of the second component of the SVD analysis of the spectral changes are also shown (open circles). (c) Temperature dependence of the amplitude of the quaternary relaxation. Symbols and analysis are identical with those in panel b. In panels b and c the amplitudes are normalized to the spectral changes at 20 °C.

Discussion

The "spectral surface" in Figure 3 shows that maximum photodissociation of the carbon monoxide complex of trout Hb I at room temperature produces a deoxy – CO difference spectrum that decays almost entirely in a single phase with a time constant of about 10 ms. This time constant is characteristic of the rate of bimolecular binding of carbon monoxide to the T state (Brunori et al., 1980). Because of the high sensitivity of our nanosecond spectrometer, however, it is possible not only to observe processes that produce small deviations from this simple behavior but also to characterize the kinetics of these processes in some detail. By using singular value decomposition to filter the data, we have been able to observe both geminate ligand rebinding and spectral changes of the deoxyheme photoproduct. When analyzed in terms of a sum of exponentials, 3 additional relaxations are observed at room temperature, with relaxation times of about 50 ns, 2 μs, and 20 μs. All 3 relaxations contain contributions from both ligand rebinding and deoxyheme spectral changes (Figure 7). In partial photolysis experiments the bimolecular rebinding regime becomes more complex (Figure 5), and additional relaxations are observed at about 400 μs, 1 ms, and 3 ms (Figure 6, Table II). Our problem is to assign these relaxations to specific molecular processes. We first briefly consider the geminate rebinding results and then discuss in some detail the deoxyheme spectral changes and the characterization of the kinetics of the R → T quaternary conformational change.

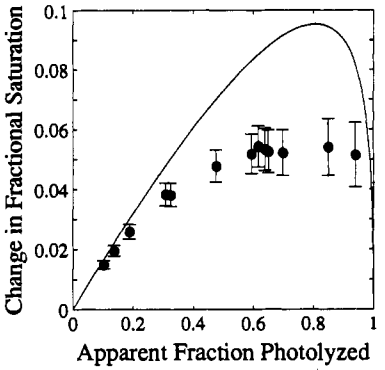

FIGURE 9: Comparison of the apparent change in fractional saturation observed in relaxation I as a function of the apparent fraction of heme–CO complexes photolyzed (filled circles) (data from Figure 7a) with the change predicted from eq 10 with no geminate rebinding (solid curve) [i.e. $[f(0,I) - f(\infty,I)]$ versus $f(0,I)$ for $k = 0$]. The largest part of the error arises from the uncertainty in the shape of the deoxyheme spectral change (Figure 7b).

(I) Photoselection and Rotational Diffusion Can Account for Most of the Change in Apparent Fractional Saturation in the Geminate Rebinding Regime. Because the apparent change in saturation accompanying relaxation I is small, the analysis of the geminate ligand rebinding in this relaxation is complicated by the effects of photoselection and rotational diffusion. It is known from polarized absorption studies on single crystals that the hemes in hemoglobin behave as nearly perfect planar absorbers of linearly polarized light at both the excitation and probe wavelengths (Makinen & Eaton, 1973; Hofrichter & Eaton, 1976; Eaton & Hofrichter, 1981). That is, there is no absorption of light polarized perpendicular to the heme plane and equal absorption of light polarized parallel to all directions in the heme plane. With our instrument both the excitation and probe pulses are linearly polarized and their electric vectors are parallel. As a result, unphotolyzed heme–CO complexes are preferentially oriented with their porphyrin planes perpendicular to the electric vector of the probe pulse. Rotational diffusion therefore results in an apparent increase in saturation that can be misinterpreted as geminate ligand rebinding. The rotational correlation time of hemoglobin is about 30 ns at 20 °C,[3] which is comparable to the observed relaxation time of 50 ns, so that rotational diffusion can contribute to the ligand rebinding observed in relaxation I. The amplitude data suggest that it makes a major contribution.

Figure 9 shows the apparent change in fractional saturation as a function of the apparent fraction photolyzed. Also plotted in Figure 9 is a theoretical curve, calculated for δ-function light pulses, for the case in which there is no geminate rebinding from the equation (Ansari et al., unpublished work):

$$f(t,I) = [(ke^{-(k+k')t} + k')/(k + k')]\left[1 - (1/2)\int_0^{\pi} e^{-I\sin^2\theta} \sin\theta \, d\theta - (1/4)e^{-t/\tau_R}\left(\int_0^{\pi} e^{-I\sin^2\theta} \sin\theta \, d\theta - 3\int_0^{\pi} e^{-I\sin^2\theta} \cos^2\theta \sin\theta \, d\theta\right)\right] \quad (10)$$

where $f(t,I)$ is the ratio of the spectral amplitude at time $t > 0$ produced by excitation with a δ-function laser pulse of finite intensity to the spectral amplitude immediately after a δ-function laser pulse of infinite intensity; k is the rate constant for geminate ligand rebinding; k' is the rate constant (or sum of rate constants) for all processes that compete with ligand rebinding; τ_R is the rotational correlation time; I contains the product of the integrated laser intensity, the extinction coefficient, and the quantum yield; and θ is the angle between the electric vector of the linearly-polarized light and the normal to the heme plane. The theoretical curve lies above the data. Since the rotational correlation time at 20 °C is only about 3 times greater than the width of the laser pulses, significant rotational diffusion takes place during the excitation pulse and the amplitudes predicted by eq 10 are expected to be too large.[4] The present data do not have sufficient information to quantitate the relative contributions of rotational diffusion and geminate rebinding to the observed change in fractional saturation. An accurate description of the ligand rebinding in relaxation I will require experiments in which isotropic spectra are calculated from measurements with the electric vector of the linearly polarized probe pulse oriented both perpendicular and parallel to the electric vector of the excitation pulse.

Two considerations suggest that geminate recombination is responsible for at least a few percent of the change in apparent saturation. First, the observed relaxation time (50 ns) is significantly longer than the rotational correlation time. Second, analysis of the relation between geminate and bimolecular rebinding for human hemoglobin and myoglobin suggests that there should be significant geminate rebinding in trout hemoglobin. In human hemoglobin the geminate yield is proportional to the bimolecular binding rates for the R and T states (Murray et al., 1988a), and in myoglobin the geminate yields for carbon monoxide and oxygen also scale with their bimolecular rates (Henry et al., 1983). Assuming that the bimolecular rate is the product of the rate of entry of the carbon monoxide into the protein and the geminate yield, the entry rate is calculated to be 1.5 (±0.4) × 10^7 M^{-1} s^{-1} for hemoglobin (Murray et al., 1988a) and 1.7 (±0.3) × 10^7 M^{-1} s^{-1} for myoglobin (Henry et al., 1983). If we assume the same entry rate for trout hemoglobin and assign relaxation IV to the R-state bimolecular rebinding rate, this semiempirical approach predicts a geminate yield of $(2.7 \times 10^6)/(1.5 \times 10^7)$ = 18%.[5] These considerations suggest that both rotational

[3] By use of a dry molecular weight of 64.4K and a density of 1.3 g/cm³, the molecular volume of hemoglobin is 8.2 × 10^{-20} cm³, and the radius of the equivalent sphere is 27 Å. Assuming that a single layer of water of thickness 3.0 Å is tightly bound to the surface of the protein (Venable & Pastor, 1988), the effective volume of the equivalent sphere is 11.3 × 10^{-20} cm³. With this hydrated volume the rotational correlation time of 28 ns is calculated for a sphere in water of 0.01 P at 20 °C by using the formula: $\tau_R = 1/6D_R = \eta V/kT$. This value is to be compared with the experimental values of 26 ± 2 ns at 20 °C from electron spin resonance measurements on spin-labeled hemoglobin (McCalley et al., 1972), 28 ns at 25 °C from dielectric relaxation measurements (Oncley, 1938), and 39 ± 7 ns at 31 °C from nuclear magnetic resonance (NMR) longitudinal relaxation times of the α-carbon envelopes (Gilman, 1979). In the NMR measurements the 1.8-fold increase in solution viscosity produced by the high (8–9 mM in heme) hemoglobin concentrations (Ross & Minton, 1977) should significantly increase the rotational correlation time. A rotational correlation time of 14.5 ns at 20 °C has been reported from fluorescence depolarization measurements on apohemoglobin reconstituted with the fluorescent dye 1-anilino-8-naphthalenesulfonate (Stryer, 1965), and a value of 23 ± 1 ns was reported at 10 °C from time-differential perturbed γ–γ angular correlations in apohemoglobin reconstituted with indium protoporphyrin IX (Marshall et al., 1983). These lower values probably result from substantial dissociation of tetramers into dimers in these reconstituted hemoglobins.

[4] An increase in the extent of rotational diffusion within the excitation pulse could also explain part of the decrease in the apparent change in fractional saturation with increasing temperature (Figure 8b). The rotational correlation time decreases from 50 ns (about 5 times the pulse width) at 2 °C to 10 ns (about the same as the pulse width) at 65 °C (see footnote 2).

diffusion and geminate rebinding contribute to the apparent change in ligand saturation observed in relaxation I.

There is a small amount of ligand rebinding in relaxation II, which is about 2% of the total rebinding at all degrees of photolysis (Figure 7c). It is assumed to arise from geminate rebinding because the corresponding bimolecular rate would be very high (5×10^8 M^{-1} s^{-1}) and its amplitude (Figure 6b) is almost linearly proportional to the apparent fraction photolyzed, unlike the bimolecular rebinding relaxations at longer times (Figure 6d–g). As pointed out earlier, above 20 °C the total spectral changes are so small that only a single relaxation is required to fit the data. Our tentative interpretation of these results is that the single relaxation above 20 °C corresponds to a mixture of relaxations I and II at 20 °C and below. As the temperature increases, less of relaxation I is resolved because the relaxation times for rotational diffusion and geminate recombination become comparable to or shorter than the pulse width.

(II) Amplitude Data Indicate That both the $R_0 \rightarrow T_0$ and $R_1 \rightarrow T_1$ Quaternary Conformational Changes Occur in the 20-μs Relaxation. Our principal objective in this work has been to characterize the kinetics of the quaternary conformational changes. This has been made difficult by the fact that the associated spectral changes are very small, representing only 8% of the total spectral change due to ligand rebinding. The total spectral change for the deoxyhemes in the first 3 relaxations is, moreover, about 2.5 times smaller than the deoxyheme spectral changes observed over the same time period in human hemoglobin (Hofrichter et al., 1983, 1985; Murray et al., 1988a). Indeed no deoxyheme spectral changes have previously been observed in either kinetic or equilibrium experiments on trout hemoglobin. In spite of this limitation we have been able to describe the kinetics of the quaternary conformational change in considerable detail.

Before beginning this discussion, we should briefly comment on the relation between the deoxyheme spectral changes and the protein conformational changes. Because of the complex nature of the Soret band of deoxyhemes, with a manyfold electronically degenerate ground state (Eaton et al., 1978; Eaton & Hofrichter, 1981; Murray et al., 1988b), and the lack of a complete theory for the Soret line shape [see, however, Srajer et al. (1986)], it is not possible to use theoretical arguments to relate structure and spectra. Some insight can be gained, however, by empirical comparison of the spectra with X-ray data. By comparing the spectral changes in human hemoglobin for the quaternary conformational change and the tertiary conformational changes within the R and T quaternary structures with the detailed X-ray results for the same structural changes, we have previously proposed that the deoxyheme spectral changes arise from changes in the position of the iron atom relative to the heme plane (Murray et al., 1988b). If this proposal is correct, then the deoxyheme spectrum reflects the conformation of the surrounding protein via its effect on the iron position (Henry et al., 1985). This interpretation of the spectral change would suggest, but by no means require, that its magnitude be monotonic in the magnitude of the surrounding protein conformational change.[6]

In the following discussion we shall equate deoxyheme spectral changes with protein conformational changes. Since the molecule is in the R state prior to photodissociation, but almost all bimolecular rebinding in maximum photolysis experiments occurs with a T-state rate at about 10 ms (Figure 4), the R → T conformational changes must be occurring on a submillisecond time scale. Our problem is to determine which of the first three relaxations corresponds to quaternary conformational changes. The results of the partial photolysis experiments provide the answer.

If each subunit in the hemoglobin tetramer responded independently to ligand photodissociation by undergoing a change in tertiary conformation which does not alter the spectra of neighboring subunits, then the amplitude of the associated change in the spectra of the deoxyhemes would be expected to scale linearly with the fraction of photolyzed heme–CO complexes. In contrast, the amplitude of the deoxyheme spectral change associated with quaternary conformational changes is expected to scale nonlinearly with the fraction photolyzed because the fraction of tetramers in ligation states that switch from R to T (see Figure 2) is a highly nonlinear function of the fraction photolyzed. We assume that the deoxyheme spectral change for a given partially liganded tetramer is proportional to the product of the number of deoxyhemes and the probability that this species switches to the T conformation. To use the spectral amplitudes to assign the spectral relaxations, we must know both these probabilities and the distribution of partially liganded tetramers in the photoproduct population which exists prior to each relaxation.

We have considered two extreme cases. If the probability of photolysis of each heme of a tetramer were uncorrelated, which would occur if the rotational correlation time were much shorter than the pulse width, the distribution of liganded tetramers would be binomial. In this case $[R_i]$, the relative concentration of the R-state tetramer with i ligands bound, is the coefficient of λ^i in the binomial expansion of $(1 - y + \lambda y)^4$, i.e.

$$\sum_{i=0}^{4} \lambda^i [R_i] = (1 - y + \lambda y)^4 \qquad (11)$$

or

$$[R_i] = [4!/i!(4 - i)!] y^i (1 - y)^{4-i} \qquad (12)$$

where y is the fractional saturation with ligand. Use of a binomial distribution assumes that all of the increase in saturation results from geminate rebinding to equivalent hemes. In the second case we recognize that the distribution of photoproduct species is no longer binomial when the rotational correlation time becomes comparable to the pulse width.

[5] The bimolecular rebinding regime of trout hemoglobin is complex (Figures 5 and 6), and we have not yet fully analyzed it. At the lowest degrees of photolysis, where no switching to the T state occurs, as evidenced by the lack of any amplitude of the T-state rebinding phase (relaxation VII in Figure 6, Table II), the bimolecular rebinding occurs mainly in two phases of roughly equal amplitudes with relaxation rates of 2.7×10^3 s^{-1} and 6.8×10^2 s^{-1} (relaxations IV and V in Figure 6). One simple interpretation of these relaxations is that they correspond to sequential bimolecular rebinding to the R state, first to α hemes and then to β hemes, or vice versa. With this interpretation, the predicted geminate yield for relaxation I, ignoring the small amount of geminate rebinding in relaxation II, is $(1/2)[({}^{\alpha}k_{on}/{}^{\alpha}k_{entry}) + ({}^{\beta}k_{on}/{}^{\beta}k_{entry})] = (1/2)[(2.7 \times 10^6)/(1.5 \times 10^7) + (6.7 \times 10^5)/(1.5 \times 10^7)] = 11\%$. We should also point out that the faster rate of 2.7×10^6 M^{-1} s^{-1} is somewhat slower than the previously reported rate of 5.1×10^6 M^{-1} s^{-1} under similar conditions (Brunori et al., 1980) (the free carbon monoxide concentration was 0.1 mM instead of the 1 mM of the present experiments, and the phosphate concentration was 0.2 M instead of 0.1 M).

[6] In human Hb the amplitude of the spectral change per deoxyheme undergoing the R → T transition is about 3 times greater than the sum of the spectral amplitudes for the two prior tertiary conformational changes (Hofrichter et al., 1985). These amplitudes are consistent with the X-ray results which show that the tertiary conformational change between the liganded and deoxy subunits within the R quaternary structure is smaller than the tertiary conformational change associated with the R to T transition (Perutz et al., 1987; Murray et al., 1988b).

Because the four hemes of hemoglobin are roughly parallel (Eaton & Hofrichter, 1981), photolysis by a linearly polarized pulse biases the population of tetramers toward molecules in which all four heme–CO complexes have been photodissociated and molecules in which none have been photodissociated. When the rotational correlation time is much longer than the pulse width, the relative population of each molecular species can be obtained by using the following simple generalization of eq 11:

$$\sum_{i=0}^{4}\lambda^i[R_i] = (1/4\pi)\int_0^{2\pi} d\phi \int_0^{\pi} \sin\theta\, d\theta \prod_{n=1}^{4}(1 - P_n + \lambda P_n) \quad (13)$$

where the probability, P_n, that the nth heme–CO complex is not photodissociated (which is analogous to y in eqs 11 and 12) is

$$P_n = \exp\{-I[1 - (\cos\theta\cos\alpha_n + \sin\theta\sin\phi\cos\beta_n + \sin\theta\cos\phi\cos\gamma_n)^2]\} \quad (14)$$

Here $\cos\alpha_n$, $\cos\beta_n$, and $\cos\gamma_n$ are the direction cosines of the normal to the nth heme plane relative to an arbitrary axis system, taken here to be the axes of the human oxyhemoglobin crystal from which the direction cosines were calculated. The integration over the polar coordinates, θ and ϕ, which define the orientation of the electric vector of the linearly polarized light in the same axis system, results from the initially isotropic distribution of tetramer orientations. If the excitation pulse is described by a δ-function, the effects of photoselection are large enough to account for all of the apparent ligand rebinding in relaxation I. For this case we therefore assume that there is no geminate rebinding, and all of the apparent increase in saturation results from rotational diffusion.

Figure 10a shows the predicted dependence of the amplitudes of deoxyheme spectral changes for each ligation state on the fraction of deoxyhemes. The relative populations of the photoproduct species at each fractional saturation are calculated from eqs 12 and 13. The probability that each species switches from R to T is assumed to be the equilibrium probability. The allosteric parameters in Figure 2 predict that virtually all R_0 and R_1 molecules switch to T at equilibrium, but only 62% of R_2 molecules and 3% of R_3 molecules switch. The shape of the curve is very different for each ligation state. The predicted amplitudes for the $R_2 \rightarrow T_2$ and $R_1 \rightarrow T_1$ transitions show maxima at intermediate levels of photolysis, while the amplitude for the $R_0 \rightarrow T_0$ transition increases cooperatively with increasing photolysis. The calculations assume that the spectral change per deoxyheme for each process is the same for all ligation states and that there is no competitive ligand rebinding. Competitive ligand rebinding decreases the amplitudes of the deoxyheme spectral changes.

Figure 10b shows the amplitudes of the spectral changes for the first three relaxations. The amplitude of the spectral change in relaxation I increases rapidly at low fractions of deoxyhemes and then appears to saturate. As discussed above, this nonlinear dependence can be attributed to the contribution of rotational diffusion to the apparent change in fractional saturation observed in this relaxation. The amplitude of the spectral change in relaxation II at about 2 μs is almost linear in the fraction of deoxyhemes. In contrast, the amplitude of the deoxyheme spectral change in relaxation III at 20 μs increases nonlinearly and cooperatively with the fraction of deoxyhemes. These results clearly point to the deoxyheme spectral change of relaxation III at 20 μs as containing the $R_0 \rightarrow T_0$ quaternary transition and indicate that the deoxyheme spectral changes of relaxations I at 50 ns and II at 2

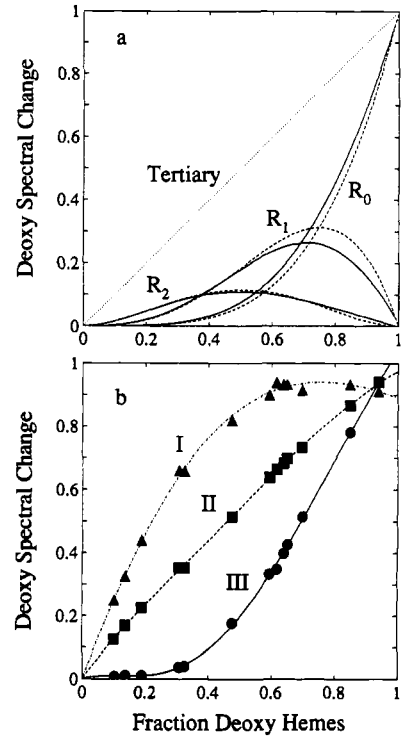

FIGURE 10: Predicted populations of partially liganded molecules which switch from R to T and observed amplitudes of relaxations I–III at 20 °C. (a) The fraction of each species which is expected to undergo a quaternary change from R to T is calculated from the thermodynamic analysis of Barisas and Gill (1979) by using both a binomial (dashed curve) and a photoselected (continuous curve) distribution of liganded species. The equilibrium allosteric parameters, L_0 = 3280 and c = 0.022 (Barisas & Gill, 1979), predict that 99.97% [$=L_0/(L_0 + 1)$] of R_0 molecules will switch to T_0 at equilibrium, 98.6% [$= L_0c/(L_0c + 1)$] of R_1 molecules will switch to T_1, and 61.4% [$= L_0c^2/(L_0c^2 + 1)$] of R_2 molecules will switch to T_2. The dotted line indicates that for tertiary conformational changes the amplitude of the spectral change is expected to be linear in the fraction of deoxyhemes (in the absence of any spectroscopic heme–heme interaction). (b) Comparison of the normalized amplitudes of spectral changes which take place in relaxations I–III (data from Figure 6a–c).

μs correspond to tertiary conformational changes within the R quaternary structure.

There is, however, a significant deviation of the data in Figure 10b from the theoretical curve for zero-liganded molecules in Figure 10a. The most likely explanation for this deviation is that singly liganded molecules are switching to the T conformation in the 20-μs relaxation as well. Figure 11 shows that there is very close agreement between the data and the theoretical curve in which both R_0 and R_1 molecules are switching in the 20-μs relaxation. From this result we conclude that both zero-liganded and singly liganded molecules undergo the R to T quaternary transition in the 20-μs relaxation at 20 °C [see Marden et al. (1986) for a similar analysis of single-wavelength data on human hemoglobin].

Support for the assignment of relaxation III to the quaternary change for zero-liganded and singly liganded molecules comes from the finding that the amplitude of relaxation VII shows almost identical dependence on the fraction of deoxyhemes (Figure 11). Relaxation VII corresponds to the slow rebinding phase with a bimolecular rate characteristic of the T state. The close similarity of the two curves suggests that the conformational change in relaxation III produces hemes that rebind with a T-state rate.

Although the observed and predicted amplitudes for the deoxyheme spectral change as a function of the apparent degree of photolysis agree extremely well (Figure 11), it is not

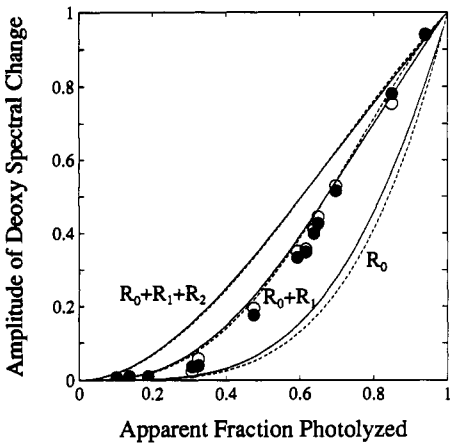

FIGURE 11: Comparison of observed and calculated amplitudes of deoxyheme spectral change in the quaternary transition (relaxation III) at 20 °C. The filled circles are the deoxyheme spectral changes for relaxation III (rank 1 component from Figure 6c), and the open circles are the amplitudes of the slow (T-state) bimolecular rebinding phase (rank 1 component of Figure 6g). The curves depict the fraction of deoxyhemes which are in tetramers that will switch to T at equilibrium plotted as a function of the fraction of deoxyhemes prior to relaxation III: The continuous curve is for the photoselected distribution, and the dashed curve is for the binomial distribution. Three cases are presented: one in which only R_0 molecules switch, one in which $R_0 + R_1$ molecules switch, and one in which $R_0 + R_1 + R_2$ molecules switch.

possible to conclude from this result that the $R_0 \rightarrow T_0$ and $R_1 \rightarrow T_1$ rates are identical. Systematic deletion of data sets from the partial photolysis experiments shows that the relaxation rate decreases as the degree of photolysis decreases, indicating that the $R_1 \rightarrow T_1$ rate is slower than the $R_0 \rightarrow T_0$ rate by at least a factor of 2. It is difficult to place a precise upper limit on the ratio of the two rates. The rate of relaxation II, which shows a linear dependence of the amplitude on degree of photolysis, is about 10 times faster than the rate of relaxation III, and the rate of relaxation IV, which shows a maximum amplitude at 50% photolysis, is about 20 times slower (Table II). It is therefore unlikely that the $R_1 \rightarrow T_1$ rate is slower than the $R_0 \rightarrow T_0$ rate by a factor of more than 5–10.

(III) Comparison of Equilibrium and Activation Parameters Indicates That the Transition State Is Much More R-like than T-like. Having assigned the 20-μs relaxation to the quaternary conformational change, we can now discuss the effect of temperature on the spectral amplitude and rate constant for the $R_0 \rightarrow T_0$ transition. In the experiments carried out at the maximum degree of photolysis at 20 °C, the contribution of $R_1 \rightarrow T_1$ to the quaternary relaxation is only about one-fourth that of $R_0 \rightarrow T_0$. Since this fraction decreases with increasing temperature as a result of the decreasing geminate yield, we ignore its contribution in evaluating the temperature dependence of the $R_0 \rightarrow T_0$ rate constant and spectral amplitude. We first discuss the temperature dependence of the spectral amplitude.

Figure 8c shows that there is a marked decrease in the amplitude of the deoxyheme spectral change in the quaternary relaxation with increasing temperature. The allosteric equilibrium parameters, extrapolated from lower temperatures, suggest that this decrease cannot be simply the result of a decrease in the fraction of deoxyhemes in tetramers that are switching from R to T (Figure 12b). The equilibrium constant for the quaternary transition has a large temperature dependence (Barisas & Gill, 1979), so that at the high temperatures a significant fraction of fully liganded tetramers is in the T state, and even larger fractions of the zero-liganded and singly liganded tetramers are in the R state. Nonetheless, the predicted decrease in the amplitude of the R to T spectral change, shown in Figure 12b, is much too small to account for the observed decrease in the amplitude of the deoxyheme spectral change with increasing temperature. Since a significant effect is predicted from the equilibrium populations, however, we have used these predictions to correct the observed spectral amplitudes (Figure 8c) for the fraction of deoxyhemes in tetramers that are switching from R to T. The results are shown in Figure 12b.

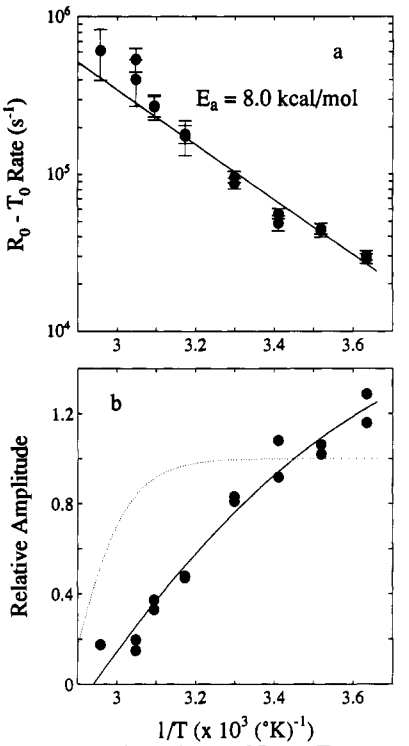

FIGURE 12: Temperature dependence of $R_0 \rightarrow T_0$ rate constant and amplitude of the deoxyheme spectral change. (a) Arrhenius plot of the $R_0 \rightarrow T_0$ rate constant. The $R_0 \rightarrow T_0$ rate constant was obtained by correcting the observed relaxation rate for the $T_0 \rightarrow R_0$ rate. At high temperatures a significant fraction of zero-liganded molecules are in the R state at equilibrium (see panel b). The effective rate constant is then the sum of the rate constants for $R_0 \rightarrow T_0$ and $T_0 \rightarrow R_0$, from which the rate constant for $R_0 \rightarrow T_0$ can be calculated by using the value of L_0 from thermodynamic studies (Barisas & Gill, 1979). No correction for competitive bimolecular ligand rebinding was made because it is so small. Only about 3% of the total ligand rebinding occurs in relaxation III at maximum photolysis at 20 °C, and this fraction decreases as the temperature increases (Figure 8c). The straight line is the least-squares fit to the data, with weighting of the data points according to the reciprocal of the relative errors. The activation energy, calculated from the slope, is 8.0 ± 0.3 kcal/mol. The relative errors increase with increasing temperature because the amplitude of the spectral change decreases. (b) Amplitude of deoxyheme spectral change associated with the R → T transition. The measured amplitudes have been corrected for the fraction of four-liganded molecules in the T-state prior to photodissociation and the fraction of zero-liganded molecules that remain in R at equilibrium. The dotted curve is the fraction of zero-liganded tetramers that are predicted to switch from R to T at equilibrium.

There is about a 6-fold decrease in the amplitude of the spectral change per deoxyheme as the temperature increases from 2 to 65 °C. Interpreted in terms of the relation between structural and spectral changes postulated at the beginning of this discussion, this decrease would result from a decrease in the difference between the iron displacements in the two quaternary structures. A decrease in the displacement of the iron between the R and T quaternary states would, in turn, reflect a decrease in the difference between the subunit tertiary conformations at high temperatures. This interpretation is supported by the thermodynamic data (Barisas & Gill, 1979).

Table III: Equilibrium and Kinetic Parameters for the Quaternary Structural Change of Trout Hemoglobin at 20 °C[a]

	$R_0 \rightarrow T_0$	$T_0 \rightarrow R_0$
L	3280 ± 1000	1/[3280 (±1000)]
k (s^{-1})	4.7 (±0.5) × 10^4	14 ± 5
ΔG (kcal/mol)	−4.7 ± 0.2	+4.7 ± 0.2
$\Delta G^{\ddagger}$ (kcal/mol)[b]	+10.8 ± 0.1	+15.6 ± 0.2
ΔH (kcal/mol)	−29.4 ± 2.1	+29.4 ± 2.1
$\Delta H^{\ddagger}$ (kcal/mol)	+7.4 ± 0.3	+36.8 ± 2.2
ΔS (cal mol^{-1} K^{-1})	−84.4 ± 7.2	+84.4 ± 7.2
$\Delta S^{\ddagger}$ (cal mol^{-1} K^{-1})[c]	−11.7 ± 1.0	+72.6 ± 7.5

[a] Equilibrium parameters from Barisas and Gill (1979); kinetic parameters from this work. [b] Calculated from eq 15 with $\kappa = 1$. [c] Calculated from eq 16 with $\kappa = 1$.

Extrapolating the data to high temperature, the difference in free energy between the two quaternary structures decreases from 6.2 kcal/mol at 2 °C to 0.9 kcal/mol at 65 °C (Barisas & Gill, 1979). Also the ratio of affinities decreases from 220 at 2 °C to 2 at 65 °C, in keeping with the idea that the difference in affinity arises from a difference in tertiary conformation that is reflected in the iron displacement.

The analysis of the temperature dependence of the rate constant is straightforward and leads to some very interesting conclusions. Figure 12a shows an Arrhenius plot of the $R_0 \rightarrow T_0$ rate constants, obtained from the observed relaxation rates (Figure 8a) after correcting for the small amount of competitive bimolecular ligand rebinding and, at the higher temperatures, for the $T_0 \rightarrow R_0$ rate. The activation energy (E_a) is 8.0 ± 0.3 kcal/mol. This activation energy can be used together with the rate constant to calculate the activation free energy ($\Delta G^{\ddagger}$), the activation enthalpy ($\Delta H^{\ddagger}$), and the activation entropy ($\Delta S^{\ddagger}$) from transition-state theory (TST) by using the equations (Steinfeld et al., 1989):

$$k = \kappa k^{TST} = \kappa(k_B T/h)e^{-\Delta G^{\ddagger}/RT} \quad (15)$$

$$k = \kappa(k_B T/h)e^{\Delta S^{\ddagger}/R}e^{-\Delta H^{\ddagger}/RT} \quad (16)$$

with

$$\Delta H^{\ddagger} = E_a - RT \quad (17)$$

These activation parameters for the $R_0 \rightarrow T_0$ quaternary conformational change can now be combined with the equilibrium parameters to obtain the enthalpy and entropy of activation for the $T_0 \rightarrow R_0$ quaternary conformational change from the thermodynamic constraints that

$$\Delta H^{\ddagger}(T_0 \rightarrow R_0) = \Delta H(T_0 \rightarrow R_0) + \Delta H^{\ddagger}(R_0 \rightarrow T_0) \quad (18)$$

and

$$\Delta S^{\ddagger}(T_0 \rightarrow R_0) = \Delta S(T_0 \rightarrow R_0) + \Delta S^{\ddagger}(R_0 \rightarrow T_0) \quad (19)$$

The equilibrium and kinetic parameters are summarized in Table III and Figure 13. In calculating the activation free energies and activation entropies, a value of unity has been assumed for the transmission coefficient, κ (see below). For the $R_0 \rightarrow T_0$ transition the activation enthalpy and activation entropy are relatively small: +7.4 kcal mol^{-1} and −12 cal mol^{-1} K^{-1}. The results are quite different for the $T_0 \rightarrow R_0$ transition. Not only are the activation parameters much larger ($\Delta H^{\ddagger}$ = +37 kcal/mol and $\Delta S^{\ddagger}$ = +73 cal mol^{-1} K^{-1}), but they are very similar to the equilibrium parameters (ΔH = +29 kcal mol^{-1} and ΔS = +85 cal mol^{-1} K^{-1}).

The similarity of the equilibrium and activation enthalpies and entropies for the $T_0 \rightarrow R_0$ transition indicates that the transition state for the quaternary structural transition between zero-liganded tetramers is much more R-like than T-like. If

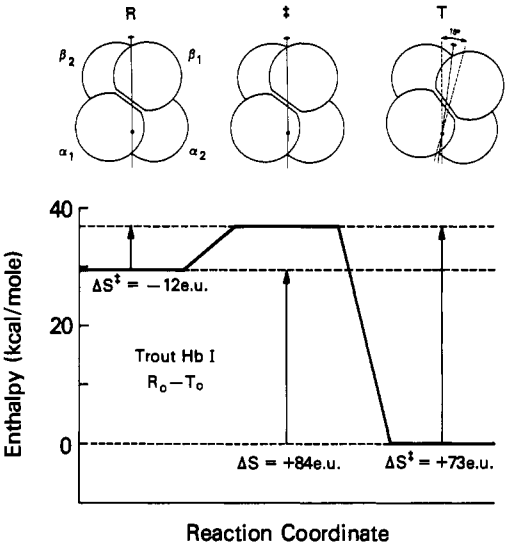

FIGURE 13: Schematic diagram of enthalpy as a function of reaction coordinate along the path from R to T (data of Table III). The similarity of the equilibrium and activation parameters for $T_0 \rightarrow R_0$ indicates that the transition state is much more R-like than T-like.

the resemblance of the transition state to the R state is structural as well as energetic, this result suggests that in the path from T_0 to R_0 the subunits have already almost completely rearranged into the R configuration when the transition state is reached, while in the path from R_0 to T_0 the subunits remain in a configuration close to R in the transition state.

It is interesting to speculate about the origin of the difference between the $T_0 \rightarrow R_0$ activation entropy and the equilibrium entropy change. Even if the transition state were completely R_0-like, the entropy of activation would in fact be expected to be lower. The difference results from the fact that the transition state is missing one vibrational degree of freedom, compared to the R_0 state, corresponding to motion along the reaction coordinate. Assuming that the energy of the vibration corresponding to the missing degree of freedom is small compared to $k_B T$, this entropy difference is given by

$$\Delta S - \Delta S^{\ddagger} = R \ln (k_B T/h\nu) \quad (20)$$

The observed entropy difference of 12 cal mol^{-1} K^{-1} could be accounted for entirely if the frequency of the vibration, ν, were 0.6 cm^{-1}, which is only slightly lower than the frequencies calculated for the lowest frequency normal modes of smaller proteins (Brooks & Karplus, 1983; Levitt et al., 1985).

The activation entropy of 73 cal mol^{-1} K^{-1} was obtained by using a value of 1 for the transmission coefficient (κ in eq 15), which corresponds to the assumption that there are no recrossings of the barrier. Values for κ less than 1 would result in more positive calculated activation entropies and could account for at least part of the deviation from the equilibrium entropy change. Values of κ less than about 0.1 (corresponding to an increase of the calculated activation entropy of greater than 4.6 cal mol^{-1} K^{-1}) are reasonable if the system is in the Kramers high friction or diffusive regime, where the rate constant would scale inversely as the first power of the viscosity. To investigate the influence of the transmission coefficient on the calculated activation entropy, we are currently studing the effect of solvent viscosity on the $R_0 \rightarrow T_0$ quaternary rate.

(IV) Concluding Remarks. The conclusion that the transition state between the R_0 and T_0 quaternary structures is much more R-like than T-like has important and interesting consequences. It predicts that adding ligands to the heme should change the free energy of the R_0 state by nearly the

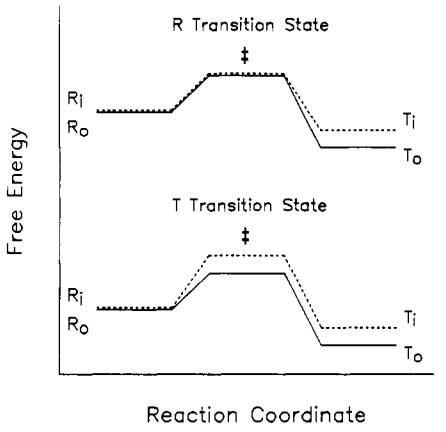

FIGURE 14: Schematic diagram showing consequences of R- and T-like transition states for ligand dependence of R–T rates. The free energy of the R state is used as a reference state. The continuous lines are the free energy levels for the molecule with no ligands bound, and the dashed lines are the free energy levels for the molecule with i ligands bound. For a completely R-like transition state the free energies of the R state and the transition state are changed by the same amount upon adding ligands. For this case all of the change in equilibrium free energy is manifested as an increase in the T → R rate, with no change in the R → T rate. For a completely T-like transition state all of the change in equilibrium free energy appears as a decrease in the R → T rate.

same amount as it changes the free energy of the transition state (Figure 14). That is, adding ligands should have a much smaller effect on the R → T rate than on the T → R rate. The results on trout Hb I are not yet clear on this point. Although $R_1 \rightarrow T_1$ is slower than $R_0 \rightarrow T_0$, it is not yet possible to determine whether the change in the R → T rate is smaller than the change in the T → R rate calculated from the change in the equilibrium constant. There is, however, a significant body of data on human hemoglobin which confirm the prediction. We present elsewhere a comparison of the R → T rates and equilibrium constants (Eaton et al., 1991). This comparison shows not only that binding ligands to the heme, as well as binding protons to the protein, results in a much smaller effect on the R → T rate than on the T → R rates, but also that there is a linear free energy relation between the rate and equilibrium constants, i.e.,

$$\log k(R_i \rightarrow T_i) = \alpha \log L_0 c^i + \log \gamma \qquad (21)$$

and

$$\log k(T_i \rightarrow R_i) = (\alpha - 1) \log L_0 c^i + \log \gamma \qquad (22)$$

so that all 10 quaternary rates can be determined from just 4 parameters—c, L_0, α, and a scaling constant, γ (Eaton et al., 1991).

The slope of the linear free energy plot, α, may be interpreted as a measure of the position of the transition state along the reaction coordinate. For $\alpha = 0$ the transition state is completely R-like, while for $\alpha = 1$ the transition state is completely T-like. The finding of $\alpha = 0.2$ indicates that the transition state is much more R-like than T-like, suggesting that the transition state appears about 20% of the distance along the reaction path from R to T (Eaton et al., 1991). This position for the transition state may be explained by a reaction path that maximizes the buried surface area between $\alpha\beta$ dimers (Janin & Wodak, 1985; Eaton et al., 1991).

ACKNOWLEDGMENTS

We thank Robert W. Zwanzig for helpful discussions.

Registry No. CO, 630-08-0; Hb I, 9034-85-9.

REFERENCES

Ackers, G. K., & Smith, F. R. (1987) *Annu. Rev. Biochem. 16*, 583-609.
Airoldi, L., Brunori, M., & Giardina, B. (1981) *FEBS Lett. 129*, 273–276.
Arnone, A., Rogers, P., Blough, N., McGourty, J., & Hoffman, B. (1986) *J. Mol. Biol. 188*, 693–706.
Baldwin, J., & Chothia, C. (1979) *J. Mol. Biol. 129*, 175–220.
Barisas, B. G., & Gill, S. J. (1979) *Biophys. Chem. 9*, 235–244.
Binotti, I., Giovenco, S., Giardina, B., Antonini, A., Brunori, M., & Wyman, J. (1971) *Arch. Biochem. Biophys. 142*, 274–280.
Brooks, B., & Karplus, M. (1983) *Proc. Natl. Acad. Sci. U.S.A. 80*, 6571–6575.
Brunori, M. (1975) *Curr. Top. Cell Regul. 9*, 1–39.
Brunori, M., Giardina, B., Chiancone, E., Spagnuolo, C., Binotti, I., & Antonini, E. (1973) *Eur. J. Biochem. 39*, 563–570.
Brunori, M., Giardina, B., Colosimo, A., Falcioni, G., & Gill, S. J. (1980) *J. Biol. Chem. 255*, 3841–3843.
Brunori, M., Giardina, B., Colosimo, A., Coletta, M., Falcioni, G., & Gill, S. J. (1982) in *Hemoglobin and Oxygen Binding* (Ho, C., Eaton, W. A., Collman, J. P., Gibson, Q. H., Leigh, J. S., Jr., Margoliash, E., Moffat, K., & Scheidt, W. R., Eds.) pp 410–412, Elsevier, New York.
Cho, K. C., & Hopfield, J. J. (1979) *Biochemistry 18*, 5826–5833.
Colosimo, A., Coletta, M., Falcioni, G., Giardina, B., Gill, S. J., & Brunori, M. (1982) *J. Mol. Biol. 160*, 531–543.
Dickerson, R. E., & Geis, I. (1983) *Hemoglobin*, Benjamin/Cummings, London.
Eaton, W. A., & Hofrichter, J. (1981) *Methods Enzymol. 76*, 175–261.
Eaton, W. A., Hanson, L. K., Stephens, P. J., Sutherland, J. C., & Dunn, J. B. R. (1978) *J. Am. Chem. Soc. 100*, 4991–5003.
Eaton, W. A., Henry, E. R., & Hofrichter, J. (1991) *Proc. Natl. Acad. Sci. U.S.A.* (in press).
Ferrone, F. A., & Hopfield, J. J. (1976) *Proc. Natl. Acad. Sci. U.S.A. 73*, 4497–4501.
Ferrone, F. A., Martino, A. J., & Basak, S. (1985) *Biophys. J. 48*, 269–282.
Giacometti, G. M., Giardina, B., Brunori, M., Giacometti, G., & Rigatti, G. (1976) *FEBS Lett. 62*, 157–160.
Gilman, J. G. (1979) *Biochemistry 18*, 2273–2279.
Henry, E. R., & Hofrichter, J. (1991) *Methods Enzymol.* (in press).
Henry, E. R., Sommer, J., Hofrichter, J., & Eaton, W. A. (1983) *J. Mol. Biol. 166*, 443–451.
Henry, E. R., Levitt, M., & Eaton, W. A. (1985) *Proc. Natl. Acad. Sci. U.S.A. 82*, 2034–2088.
Hofrichter, J., & Eaton, W. A. (1976) *Annu. Rev. Biophys. Bioeng. 5*, 511–560.
Hofrichter, J., Sommer, J. H., Henry, E. R., & Eaton, W. A. (1983) *Proc. Natl. Acad. Sci. U.S.A. 80*, 2235–2239.
Hofrichter, J., Henry, E. R., Sommer, J. H., Deutsch, R., Ikeda-Saito, M., Yonetani, T., & Eaton, W. A. (1985) *Biochemistry 24*, 2667–2679.
Hofrichter, J., Henry, E. R., & Lozier, R. H. (1989) *Biophys. J. 56*, 693–706.
Hopfield, J. J., Shulman, R. G., & Ogawa, S. (1971) *J. Mol. Biol. 61*, 425–443.
Janin, J., & Wodak, S. J. (1985) *Biopolymers 24*, 509–526.

Levitt, M., Sander, C., & Stern, P. S. (1985) *J. Mol. Biol. 181*, 423-447.
Liddington, R., Derewenda, Z., Dodson, G., & Harris, D. (1988) *Nature 331*, 725-728.
Luisi, B., & Shibayama, N. (1989) *J. Mol. Biol. 206*, 723-736.
Makinen, M. W., & Eaton, W. A. (1973) *Ann. N.Y. Acad. Sci. 206*, 210-222.
Makinen, M. W., & Eaton, W. A. (1974) *Nature 247*, 62-64.
Marden, M. C., Hazard, E. S., III, & Gibson, Q. H. (1986) *Biochemistry 25*, 7591-7596.
Marshall, A. G., Lee, K. M., & Martin, P. W. (1983) *J. Chem. Phys. 78*, 1528-1532.
Martino, A. J., & Ferrone, F. A. (1989) *Biophys. J. 56*, 781-794.
Mauer, R., Vogel, J., & Schneider, S. (1987) *Photochem. Photobiol. 26*, 255-262.
McCalley, R. C., Shimshick, E. J., & McConnell, H. M. (1972) *Chem. Phys. Lett. 13*, 115.
Monod, J., Wyman, J., & Changeux, J.-P. (1965) *J. Mol. Biol. 12*, 88-118.
Murray, L. P., Hofrichter, J., Henry, E. R., Ikeda-Saito, M., Kitagishi, K., Yonetani, T., & Eaton, W. A. (1988a) *Proc. Natl. Acad. Sci. U.S.A. 85*, 2151-2155.
Murray, L. P., Hofrichter, J., Henry, E. R., & Eaton, W. A. (1988b) *Biophys. Chem. 29*, 63-76.
Nagle, J. F., Bhattacharjee, S. M., Parodi, L. A., & Lozier, R. H. (1983) *Photochem. Photobiol. 38*, 331-339.
Oncley, J. L. (1938) *J. Am. Chem. Soc. 60*, 1115-1123.
Perutz, M. F. (1970) *Nature (London) 228*, 726-734.
Perutz, M. F. (1987) in *The Molecular Basis of Blood Diseases* (Stamatoyannopoulos et al., Eds.) pp 126-162, W. B. Saunders, Philadelphia.
Perutz, M. F., Fermi, G., Luisi, B., Shaanan, B., & Liddington, R. C. (1987) *Acc. Chem. Res. 20*, 309-321.
Ross, P. D., & Minton, A. P. (1977) *Biochem. Biophys. Res. Commun. 76*, 971-976.
Sawicki, C. A., & Gibson, Q. H. (1976) *J. Biol. Chem. 251*, 1533-1542.
Sawicki, C. A., & Gibson, Q. H. (1977) *J. Biol. Chem. 252*, 5783-5788.
Shrager, R. I. (1986) *Chem. Intell. Lab. Systems 1*, 59-70.
Shulman, R. G., Hopfield, J. J., & Ogawa, S. (1975) *Q. Rev. Biophys. 8*, 325-420.
Srajer, V., Schomacker, K. T., & Champion, P. M. (1986) *Phys. Rev. Lett. 57*, 1267-1270.
Steinfeld, J. I., Francisco, J. S., & Hase, W. L. (1989) *Chemical Kinetics and Dynamics*, Prentice Hall, Englewood Cliffs, NJ.
Stryer, L. (1965) *J. Mol. Biol. 13*, 482-495.
Su, C., Park, Y. D., Lui G.-Y., & Spiro, T. G. (1989) *J. Am. Chem. Soc. 111*, 3457-3459.
Venable, R. M., & Pastor, R. W. (1988) *Biopolymers 27*, 1001-1014.
Wyman, J., Gill, S. J., Noll, L., Giardina, B., Colosimo, A., & Brunori, M. (1977) *J. Mol. Biol. 109*, 195-205.

In Vitro Folding Pathway of Phage P22 Tailspike Protein†

Albert Fuchs, Claudia Seiderer,‡ and Robert Seckler*
Universität Regensburg, Institut für Biophysik und Physikalische Biochemie, Universitätsstrasse 31, D-8400 Regensburg, Federal Republic of Germany

Received January 2, 1991; Revised Manuscript Received March 20, 1991

ABSTRACT: The intracellular chain folding and association pathway of the thermostable, trimeric phage P22 tailspike endorhamnosidase has been the subject of a previous detailed study employing temperature-sensitive folding mutants. Recently, reconstitution of native tailspikes from completely unfolded polypeptides has been accomplished, providing a model system to compare protein folding pathways in vivo and in vitro. The in vitro reconstitution pathway of the protein after dilution from guanidine hydrochloride or acid–urea solutions at 10 °C was characterized by spectroscopic and hydrodynamic techniques, and may be summarized as an ordered sequence of folding, association, and folding reactions. Multiphasic folding of monomers was indicated by changes in circular dichroism and fluorescence, with a rate constant of $k = 1.6 \times 10^{-3}$ s^{-1} for the slowest phase observed spectroscopically. Trimerization of structured monomers was followed by size-exclusion HPLC and was completed within 1.5 h at a protein concentration of 20 μg/mL. Although at this time trimers did not exchange subunits, they were readily dissociable by dodecyl sulfate in the cold. Formation of native, detergent-resistant trimers was only completed after 3 days of reconstitution at 10 °C. The reconstitution pathway of the tailspike protein closely resembles its intracellular maturation path. Thus, the in vitro reconstitution system, as a valid model of chain folding and association in vivo, should provide the tools to localize the steps or intermediates on the pathway that are the targets of temperature-sensitive folding mutations.

A number of cellular proteins have been described in recent years to function as folding helpers increasing the efficiency or the rate of protein folding and assembly (Ellis, 1990; Fischer & Schmid, 1990). Nevertheless, it remains generally accepted that the final three-dimensional structure a polypeptide chain assumes in a functional protein is determined by its amino acid sequence, although the rules of such structure formation have yet to be elucidated (Kim & Baldwin, 1982, 1990; Jaenicke, 1987; Kuwajima, 1989). Clues toward determining such rules may be obtained from studying the refolding and reassociation

† This work was supported by a grant from the Deutsche Forschungsgemeinschaft (Se 517/1-1) and by the Fonds der Chemischen Industrie.
* Address correspondence to this author.
‡ Present address: Universität Würzburg, Institut für Toxikologie, Versbacherstrasse 9, D-8700 Würzburg, Germany.

0006-2960/91/0430-6598$02.50/0